

MIT Open Access Articles

*Scalar Simulation and Parameterization of
Water Table Dynamics in Tropical Peatlands*

The MIT Faculty has made this article openly available. **Please share**
how this access benefits you. Your story matters.

Citation: Cobb, Alexander R. and Harvey, Charles F. 2019. "Scalar Simulation and Parameterization of Water Table Dynamics in Tropical Peatlands." *Water Resources Research*, 55 (11).

As Published: <http://dx.doi.org/10.1029/2019wr025411>

Publisher: American Geophysical Union (AGU)

Persistent URL: <https://hdl.handle.net/1721.1/140457>

Version: Author's final manuscript: final author's manuscript post peer review, without publisher's formatting or copy editing

Terms of use: Creative Commons Attribution-Noncommercial-Share Alike



Scalar simulation and parameterization of water-table dynamics in tropical peatlands

Alexander R. Cobb¹, Charles F. Harvey^{1,2}

¹Center for Environmental Sensing and Modeling, Singapore-MIT Alliance for Research and Technology, Singapore.

²Department of Civil and Environmental Engineering, Massachusetts Institute of Technology, Cambridge, Massachusetts,
USA.

Key Points:

- Hydrologic-ecosystem feedback in tropical peatlands creates large areas with a uniform topographic wetness index.
- We show simple ways to estimate transmissivity and specific yield as functions of water level at the hillslope scale in tropical peatlands.
- We show that rainfall-runoff models based on a scalar hydraulic state are especially well suited to natural tropical peatlands.

This is the author manuscript accepted for publication and has undergone full peer review but has not been through the copyediting, typesetting, pagination and proofreading process, which

Corresponding author: Alexander R. Cobb, alex.cobb@smart.mit.edu
may lead to differences between this version and the Version of Record. Please cite this article
as doi: [10.1029/2019WR025411](https://doi.org/10.1029/2019WR025411)

Abstract

Peatlands cover many low-lying areas in the tropics. Tropical peatlands are intriguing systems because of their tight coupling between hydrology and carbon storage: they accumulate carbon over thousands of years because of waterlogging, and they remain waterlogged after growing into domed shapes because peat restricts drainage. This feedback between waterlogging and landscape morphology generates landforms with special hydrologic properties that enable simplifications of standard watershed models. In natural tropical peatlands, the water table is always near the surface and infiltration is almost immediate. In addition, water-table fluctuations relative to the peat surface are remarkably uniform across tropical peatlands because these peatlands acquire shapes with a uniform topographic wetness index. In this paper, we show that because of these distinctive properties, simple hydrologic models that represent the hydraulic state of a catchment by a scalar quantity that describes total water storage are useful and physically meaningful in tropical peatlands. We demonstrate how to efficiently derive hillslope-scale parameterizations of transmissivity and specific yield as functions of water-table height for a tropical peatland from water-table, rainfall and topographic data. Our findings suggest that natural tropical peatland subcatchments could be usefully modeled as single hydrologic response units for river flow and flood forecasting.

1 Introduction

Tropical peatlands are ancient ecosystems [Morley, 2013] in which waterlogging slows decay of woody plant remains so that organic matter accumulates in deposits that can be many meters thick [Molengraaff, 1900; Anderson, 1983]. This partly decomposed organic matter (peat) accumulates over thousands of years into gently mounded landforms, or peat domes, between geographic boundaries such as hills or rivers [Anderson, 1964]. Tropical peat domes are estimated to contain at least 75 Gt of carbon [Warren *et al.*, 2017; Xu *et al.*, 2018], but much of this carbon has been released in recent years by decomposition and fire following peatland drainage for conversion to agriculture [Miettinen *et al.*, 2016; Page and Hooijer, 2016]. Because tropical peatlands store a very high mass of carbon per area—much greater than in tropical forests—conversion of tropical peatlands causes the highest greenhouse gas emissions per area of any land use, land use change or forestry activity [Warren *et al.*, 2017].

In addition, tropical peatlands lie mostly in coastal, low-lying regions that include some of the densest settlements in the islands of Southeast Asia [Center For International Earth Science Information Network–CIESIN–Columbia University, 2017; World Resources Institute, 2018]. After these peatlands are drained, the elevation of the peat surface gradually decreases from a combination of compaction, decomposition and fire [Hooijer *et al.*, 2012] at rates that exceed those of sea level rise. These swampy areas are frequently subject to flooding, which local people accommodate by building their houses on stilts [Hidayat *et al.*, 2012; Wells *et al.*, 2016]. As urban centers in tropical peatlands grow, it is increasingly important to predict storm response and assess flood risk. Peatlands, like other wetlands, can either speed up or slow down fluvial response to rainfall, depending on their position in the catchment and antecedent conditions [Acreman and Holden, 2013]. Projected increases in seasonality of rainfall in Southeast Asia [Kang *et al.*, 2019] imply increased intermittency of rainfall that could worsen flooding issues in peatlands of the region.

Tropical peatland rivers also export dissolved organic carbon (DOC). Groundwater DOC concentrations in tropical peatlands can be very high [5–6 mmol / l; Gandois *et al.*, 2013] and rivers with peatland subcatchments have among the highest DOC concentrations reported, often carrying 2–3 mmol / l DOC or more [Alkhatib *et al.*, 2007; Müller *et al.*, 2015]. Because peatlands arise in areas of heavy rainfall in the lowland tropics, the total discharge from these areas is large, and contributes to the discharge of major tropical rivers such as the Kapuas of west Borneo, the Siak of Sumatra, and the Congo [Dargie *et al.*, 2017]. Therefore, discharge from peatlands is also important because it controls large organic exports to rivers and oceans [Baum *et al.*, 2007; Moore *et al.*, 2011; Wit *et al.*, 2015].

Predictions of fire and flood risk, peat oxidation and DOC export require data describing the response of peatland water tables and discharge to rainfall. Unfortunately, data on the hydraulic properties of tropical peatlands are extremely limited. Because of danger, difficulty, and expense, vast areas of tropical peatlands in Papua, the Congo and the Americas are unlikely to be instrumented in the foreseeable future. Even the extent of tropical peatlands remains poorly known: peatlands in the Cuvette Centrale depression in the central Congo Basin, 145,500 km² in area yet only described in the scientific literature in 2017 [Dargie *et al.*, 2017], are now believed to account for 24–41% of tropical peatland area [Warren *et al.*, 2017]. To our knowledge, only four studies in the peer-reviewed literature

provide data on hydraulic conductivity or transmissivity in tropical peatlands [Takahashi and Yonetani, 1997; Kelly *et al.*, 2014; Baird *et al.*, 2017; Cobb *et al.*, 2017].

Obtaining hydraulic properties of tropical peat for modeling is problematic because most flow occurs near the peat surface, where hydraulic conductivity is very difficult to measure. Tropical peatlands are characterized by high annual rainfall and small water table elevation gradients. Most water flows through a very-high-permeability near-surface layer, driven by these small gradients, to exit the peatland into bounding rivers. Groundwater hydrographs have shown that peat hydraulic parameters vary dramatically within this layer [Hooijer, 2005; Cobb *et al.*, 2017]. These large vertical differences in permeability are important in characterizing how discharge and water-table recession change with catchment storage. On the other hand, because this layer consists of an open-structured loose matrix of woody debris, vegetation, buttresses and clay-like amorphous peat, created by large-statured, hard-wooded tropical trees or palms [Anderson, 1983; Lahteenoja *et al.*, 2009; Dommain *et al.*, 2015; Dargie *et al.*, 2017], it also has large, meter-scale heterogeneity in hydraulic properties in the horizontal direction. So, for a method to characterize peatland hydraulic parameters to be useful, it must be (1) capable of measuring the very high conductivity of the surface peat layer; (2) sensitive to centimeter-scale parameter gradients in the vertical direction; and (3) robust to meter-scale heterogeneity in hydraulic properties in horizontal directions.

Standard field methods such as pump, slug or bail tests are not appropriate to characterize peat hydraulic parameters for dome-scale hydrologic models because: (1) Piezometer tests are most sensitive to the hydraulic conductivity of the material immediately around the piezometer screen, a property that varies over orders of magnitude from one piezometer location to another; (2) Piezometer tests shift the water table up or down in the vicinity of the piezometer, allowing more or less flow through the high-conductivity surface layer and confounding the interpretation of test results; and (3) Piezometer tests induce vertical flow, even if screened across the complete peat thickness because of the high conductivity at the surface, again confounding the interpretation of the test for dome-scale horizontal conductivity. Inferring bulk conductivity of this layer from laboratory tests is also impractical: it is not clear how one could sample from the surface matrix of hardwoods, voids, and amorphous peat, nor how to obtain an effective conductivity given the complex spatial configuration of these materials [Binley *et al.*, 1989]. Yet despite the lack of data and

methods, practical decisions still need to be made about hydrologic risks and management in these peatlands.

In view of the lack of data and methods and the need for hydrologic prediction in tropical peatlands, simple lumped models have been widely used that represent the hydraulic state of large peatland areas with a single number representing their wetness or dryness [e.g., *Field et al.*, 2004; *Kurnianto et al.*, 2015; *Mezbahuddin et al.*, 2015; *Shawki et al.*, 2017; *Taufik et al.*, 2017]. We call these “scalar” models to distinguish them from models that track the distribution of moisture in catchments. Scalar models are likely to be used for decades to come in applications related to fire and flood risk and peatland management because the data needed for distributed models will not be available anytime soon in many tropical peatlands. The parameters of these models typically capture the combined effects of rainfall, evapotranspiration, local topographic gradients driving flow, and peat hydraulic properties. Therefore, parameters of such models determined for one peatland area may or may not be transferable to another peatland, even if hydraulic properties of the peat are similar, if rainfall, evapotranspiration, or topography differ.

In *Cobb et al.* [2017], we showed how the special topography of tropical peatlands allows the extraction of hydraulic parameter profiles from easily obtainable water table and rainfall data. Within a peatland, peat accumulates faster in low-lying areas where divergence of horizontal flow is slower and the water table resides higher in the soil profile, reducing decomposition. Over time, the peat surface evolves towards a shape with a uniform curvature, in which the mean water level relative to the peat surface is uniform and the rate of production of organic matter is balanced by its decomposition above the water table. The uniform curvature of the peat surface over large spatial scales, combined with approximately uniform peat hydraulic properties, can explain the strikingly uniform fluctuations of the water table that have been observed in tropical peatlands [*Hooijer*, 2005; *Cobb et al.*, 2017]. In *Cobb et al.* [2017], we used this theory to develop a method for estimating transmissivity from topographic data and the fluctuations of the water table. Because that paper focused on the morphologic evolution of tropical peatlands, it did not explore the applicability and limitations of the approach for attacking practical problems in tropical peatland hydrology.

In this paper, we show how the methods first developed in *Cobb et al.* [2017] can be used to obtain all the essential topographic and hydraulic parameters for a scalar model of trop-

ical peatland hydrology using measurements that are achievable within the severe practical constraints common in tropical peatlands. We then explore the limitations of the scalar approach and extend it to applications in discharge modeling. Our goal is not to replace higher-dimensional models [e.g., DigiBog; *Baird et al.*, 2012; *Kelly et al.*, 2014; *Baird et al.*, 2017] but to describe a method for their initial parameterization, and an alternate method for simulation where data are insufficient for distributed models. Our objectives are: (1) To show why scalar models can work better in natural tropical peatlands than in many other systems, and explain the link between the Laplacian of the peat surface elevation [*Cobb et al.*, 2017] and the topographic wetness index (TWI) of TOPMODEL [*Beven and Kirkby*, 1979]; (2) To demonstrate how hillslope-scale conductivity profiles can be calculated using topographic data and field measurements, and place conductivity estimates in the context of other peatland studies; and (3) To explore implications of scalar behavior for predictions of drying and discharge in tropical peatlands, and examine the possible effects on peak discharge if rainfall intermittency increases as projected for many tropical peatlands in the coming decades.

2 Methods

Here we describe a sequence of methods for mathematical analysis and field data collection that create a scalar hydrologic model for tropical peatlands. First, we develop an approach for calculating the Laplacian of the peat surface from topographic data and describe how we obtained the necessary data from airborne LiDAR. We then describe how we collected rainfall and water table data from our field site and present a numerical method for combining these data to construct master curves for water table rise and recession. Next, we describe how the master curves are combined with the topographic analysis to determine the peat's hydraulic parameters: depth profiles of hydraulic conductivity and specific yield.

The means for assembling the master curves and extracting hydraulic parameters were first sketched in *Cobb et al.* [2017], where they were used for simulating the morphogenesis of tropical peat domes. That study applied a scalar model based on these parameters to determine the stable peat surface Laplacian as a statistic of rainfall and evapotranspiration, but gave only brief derivations of several of the essential methods. Here we provide explicit derivations and explain the sequence of steps required to construct a scalar hydrologic model for a tropical peatland. Finally, we describe how all of these mathematical meth-

ods and data are combined to calculate a water balance, simulate discharge to rivers and study the effects of rainfall intermittency on discharge.

2.1 Topographic analysis

Tropical peat domes typically occur on interfluvies kilometers to tens of kilometers across, and are gently domed to an elevation of six to ten meters higher at the groundwater divide than at the bounding rivers [Figure 1; *Anderson, 1964; Hooijer, 2005*]. Nonetheless, each hillslope on a tropical peat dome must deliver water to bounding rivers at an average rate equal to the area of the hillslope times net precipitation. The rate of divergence of horizontal groundwater flow is governed in part by the curvature of the groundwater mound, and therefore this slight curvature is a key parameter in characterizing the hydrology of the peat dome.

A useful way to characterize the curvature of the groundwater mound is with the Laplacian of the water table. The Laplacian of an elevation is equal to the sum of its second derivative in two orthogonal directions, and if applied to the land surface, is equal to the sum of the profile and planform curvatures of digital terrain analysis [*Zevenbergen and Thorne, 1987*]. A negative Laplacian indicates a convex dome, and the larger its magnitude, the steeper the dome.

The groundwater mound in a natural peat dome has roughly the same shape as the peat surface, because the water table is within tens of centimeters of the surface everywhere [*Hooijer, 2005; Hirano et al., 2009; Cobb et al., 2017*]. Therefore we can estimate the curvature of the water table by examining the peat surface topography. However, we face a problem here because the forest floor is a dense tangle of tree buttresses, *Pandanus* rhizomes, and woody debris, creating a peat surface with a complex microtopography of depressions, or hollows, and intervening areas of higher elevations, or hummocks, on the scale of meters [*Lampela et al., 2016*]. This microtopography does not reflect the local shape of the water table, which is relatively smooth [*Ritzema et al., 2014; Cobb et al., 2017*]. Therefore, to get an estimate of the curvature of the groundwater mound, we need to somehow average out the small-spatial-scale fluctuations in the peat surface from hummocks and hollows. Here, we apply basic concepts from multivariate calculus to develop a practical method for estimating the Laplacian of the groundwater mound from topo-

graphic data in peatlands. Though the method is straightforward, as far as we know it has not been presented before, except for a brief description in *Cobb et al.* [2017].

The Divergence Theorem tells us that the peat surface Laplacian $\nabla^2 p$ integrated over a region A is equal to the normal component $\nabla p \cdot \mathbf{n}$ of the peat surface gradient ∇p , integrated along the boundary ∂A of that region

$$\iint_A \nabla^2 p \, dA = \oint_{\partial A} \nabla p \cdot \mathbf{n} \, ds \quad (1)$$

(Figure 1c).

High-resolution topographic data often do not cover entire interfluves, and even when such data are available, some boundaries of a peatland may be obscure. A useful approach then is to examine topography within flow tubes. In general, a flow tube comprises a groundwater divide (which may be a line or a point), two bounding flowlines, and a downstream contour c (Figure 1b). Conveniently, the normal component of the gradient along a groundwater divide and along a flowline are both zero, leaving only the downstream contour with a non-zero normal component of the gradient. On this downstream contour, the normal component of the gradient is equal to the magnitude of the gradient $\nabla p \cdot \mathbf{n} = |\nabla p|$, the slope in the downhill direction, because the gradient must be perpendicular to the contour (Figure 1c). So, equation (1) simplifies to

$$\iint_A \nabla^2 p \, dA = \int_c |\nabla p| \, dc \quad (2)$$

where c is a contour line segment across a flow tube (Figure 1c).

After substitution using equation (2), differentiating equation (1) with respect to enclosed area A yields an expression for the Laplacian of the surface elevation

$$\nabla^2 p = \frac{d}{dA} \int_c |\nabla p| \, dc, \quad (3)$$

and using this expression (3) the Laplacian $\nabla^2 p$ of the surface elevation can be obtained graphically by plotting the integral of the normal gradient $\int_c |\nabla p| \, dc$ taken along a contour that crosses a flow tube against the area upstream of that contour (Figure 1e). Where the plotted points form a straight line, the Laplacian is approximately uniform. The slope of a line fit to the points in the plot gives an average Laplacian in that region of the flow tube. This approach can be used for a flow tube of arbitrary size.

Note that the same flow tube-based approach for the peat surface Laplacian could be used starting from an arbitrary contour in the flow tube downstream of the groundwater divide.

If a contour below the groundwater divide is used, this has the effect of shifting the curve in Figure 1e down and to the left on its axes, without altering the slope (and the Laplacian estimate) in the region of interest.

The TWI of TOPMODEL [Beven and Kirkby, 1979] is related to the Laplacian of the surface elevation. In TOPMODEL, each catchment is modeled as having a thin soil, in which transmissivity increases exponentially with water table height, on top of an impermeable bedrock. In our approximation of tropical peatland hydrology, the surface peat corresponds to this thin soil, whereas the low-permeability deeper peat corresponds to the impermeable “bedrock.” The magnitude of the gradient in the peat surface elevation $|\nabla p|$ along a contour is the parameter $\tan \beta$ in $\text{TWI} = \log(a/\tan \beta)$, where a is the contributing area per unit contour, so the TWI is equal to the negated log of the negated Laplacian of the surface elevation

$$\text{TWI} = -\log(-\nabla^2 p). \quad (4)$$

Steeper domes shed water more readily and have larger negative Laplacians $-\nabla^2 p$, giving a lower TWI.

2.2 Topographic data

We applied our flow tube-based approach to analyze the topography of a peat dome in the Ulu Mendaram Conservation Area of the Belait District in Brunei Darussalam, on the island of Borneo (4.359863° N, 114.352252° E; Figure 2). We used aerial LiDAR data for the peat dome (Brunei Survey Department, 2009) to construct a digital terrain model (DTM) by taking the minimum last-return elevation within 20 m \times 20 m grid cells. We then smoothed the DTM (GRASS GIS 6.4.3, <http://grass.osgeo.org/>) and created a contour vector map (GDAL 2.2.4, <http://www.gdal.org/>). To create a flow tube for topographic analysis, we constructed boundary flow lines from contours using the TAPES-C algorithm [Moore and Grayson, 1991]. In this case, the flow tube appears to converge to a point (Figure 2c), but this presents no problems for the approach to topographic analysis outlined above.

As explained above, the normal component of the peat surface gradient is by definition zero along the groundwater divide (here also of zero length) and along the flowlines, so we can compute the integral around the boundary by integrating the surface elevation gradient along just the downstream contour c . We computed this integral by sampling the

magnitude of the gradient along the contour and computing the area of the flowtube upstream of the contour using a spatial database (SpatiaLite 4.2.0, <http://www.gaia-gis.it/gaia-sins/>; Figure 2e).

We selected a range of enclosed areas from 3.325 km² to 6.216 km², a region around the piezometers (Figure 2c,d), to compute the mean peat surface Laplacian as the slope of a linear regression line fit to integrated-gradient-vs-area data (Figure 2e). The slope of this fitted line provides the average Laplacian $\nabla^2 p$ of the peat surface elevation enclosed by the flow tube from the groundwater divide to that contour, or an average TWI on that portion of the contour. The region of the fit indicates a zone where peat is neither accumulating nor being lost (“stable”). Upslope of this zone (left) we found ongoing peat accumulation [Cobb *et al.*, 2017], and the downslope zone (right) is affected by river flooding (Figure 2d,e). A shift in the bounds of the region would effect the Laplacian estimate inasmuch as it alters this slope. Finally, for comparison with the TWI, we computed a TWI corresponding to the average peat surface Laplacian $\overline{\nabla^2 p}$ in the study area (equation 4).

2.3 Field data

We recorded throughfall and water-table data at the field site of our topographic analysis (Figure 2a–c) from 2012-02-07 through 2013-02-18. This site is an unlogged *Shorea albida*-dominated peat swamp forest, further described in Dommain *et al.* [2015] and Cobb *et al.* [2017]. Average rainfall at the nearby Seria and Kuala Belait weather stations was 2880 mm / y in 1947 through 2004.

The site was instrumented with throughfall gauges and piezometers using methods described in Cobb *et al.* [2017]. Four siphoning tipping-bucket rain gauges (Texas Electronics TR-525S, Dallas, Texas, USA) were installed 50 cm above the peat surface to measure throughfall, and water-table height was recorded every 20 minutes at each of 5 piezometers along a 2.5 km transect using logging pressure transducers (Solinst Levellogger Edge 3001, Solinst Canada, Georgetown, Ontario, Canada). Each transducer was suspended on a steel cable inside a piezometer constructed from a 2” PVC pipe 1.5 m in length installed to 1.4 m depth and screened at 1.3–1.45 m below the top of the casing. Piezometers were developed prior to measurement by repeatedly plunging and removing a solid rod into the piezometer tube [SurrIDGE *et al.*, 2005]. Transducer measurements were corrected for barometric fluctuations using a barometer (Solinst Barologger Gold 3001). In this paper,

we discuss data from the 4 piezometers installed in the portion of the peat dome with an equilibrium morphology and uniform water-table behavior from *Cobb et al.* [2017], which span a distance of 2 km (Figure 2c,d).

2.4 Water-table rise and recession analysis

Following *Bechtold et al.* [2014] we use “water level” ζ to refer to the elevation of the water table H relative to the peat surface p ($\zeta = H - p$; Figure 1d). It was apparent from the water level data (Figure 3b) that the water level in each of the piezometers was remarkably similar at all times [*Cobb et al.*, 2017]. Therefore, the mean water level across piezometers (height of water table above peat surface), a scalar, provides a good summary of the hydraulic state of all the piezometers along the transect. Furthermore, from a given initial water-table position, the water table appeared to recede in a strongly similar way after different storms in the time series.

To explore the similarity of the water-table response to storms and dry intervals, we first identified intervals in the throughfall data of heavy rain (storms; throughfall intensity greater than 4 mm / h) and no rain (interstorms; throughfall intensity = 0, Figure 3c). (Note that by these definitions there were some intervals of the time series that were neither storms nor interstorms.) We then explored the recession of the water table during distinct interstorms by an approach similar to the sliding strips method of *Snyder* [1939] or automated variants by other authors [*Arnold et al.*, 1995; *Heppner and Nimmo*, 2005; *Posavec et al.*, 2006]. Our method aligns the short time series of mean water level during each interstorm to create a single master water level recession curve that could be imagined as the recession of the water table from its highest level during a long, uninterrupted dry spell. Our goal was to minimize the least-squared difference in elapsed time at which the water table crossed the same level in each recession. To perform the alignment, we interpolated each recession, recorded at time intervals of 20 minutes, to a uniform 1 mm grid of water level. We then found an offset in elapsed time for each recession that minimized the mean squared difference in elapsed time for all recessions that crossed each water level, as follows.

We first re-sampled each of the J recessions with a cubic spline to obtain the times at which the recession crossed each integer multiple of a uniform step size $\Delta\zeta$. A recession could cross the same water level multiple times because of measurement noise and

near-constant water levels low in the soil profile at night. For simplicity, we replaced all distinct crossing times t at a particular water level ζ with their average \bar{t} to give distinct values (k, j, \bar{t}) where k is the water level as an integer multiple of the step size $\Delta\zeta$ and j is the recession number.

There were some short recessions at the very highest and lowest water levels that did not overlap with the rest of the recessions. We eliminated these non-overlapping recessions, leaving a single large connected component of time-versus-water-level series. We also removed water levels crossed in only one recession because these contribute no information when finding time offsets.

We then solved for a time offset Δt_j for each recession by minimizing the mean squared difference in all elapsed times at each water level, as follows. Ideally, after the offset Δt_j for a recession has been applied, the time t_{ij} at which the recession crosses each water level equals the mean time at that water level across all $J(i)$ recessions that cross the water level i

$$t_{ij} + \Delta t_j = \frac{1}{J(i)} \left(\sum_{j=1}^{J(i)} \Delta t_j + t_{ij} \right),$$

so at each discrete water level i and for each recession $j \in \{1, 2, \dots, J-1\}$ we have an equation with an unknown time offset Δt_j

$$\left(\frac{1}{J(i)} \sum_{j=1}^{J(i)} \Delta t_j \right) - \Delta t_j = t_{ij} - \frac{1}{J(i)} \sum_{j=1}^{J(i)} t_{ij}$$

giving an overdetermined system of at least one linear equation for the time offset Δt_j of each recession at each discrete water level. The prior elimination of disconnected series ensures that there is an equation at each water level, and the removal of water levels with only one series ensures that there are no trivial equations. We excluded one recession J from the unknown vector; its offset was fixed so that the mean time offset was zero at water level 0 (water table at bottom of hollows) to make the least-squares solution unique. After solving this system of equations by least squares (LU decomposition), the solution vector Δt contains the time offset for each recession that minimizes the variance among recessions in elapsed time at each water level.

In *Cobb et al.* [2017], the arbitrary horizontal offset of the master recession curve was set so that elapsed time was zero on the left edge of the recession curve plot. However, that convention has the disadvantage that the horizontal position of the recession curve is sensitive to the highest observed water level in the time series. For example, suppose we had

produced a master recession curve from July through August of 2012, when the water table was below about -5 cm. Using the convention from *Cobb et al.* [2017], the higher water level data from the later part of the year could only be added by shifting the curve from the earlier data to the right, whereas by aligning the curve through the origin the new data could be simply plotted to the left of the earlier data on the same axes. Therefore, we set the offset of the time axis so that zero time coincided with zero water level. This convention also allows data from different locations to be compared on the same axes.

We analyzed the response of the water level in the peatland to rain (Figure 4a,b) using a similar approach to the recession analysis, with water level now a function of storm depth instead of time. For each storm, we calculated the total storm depth from throughfall data and determined the mean water level across piezometers at the beginning and end of the storm. Rain storms did not arrive simultaneously at throughfall gauges and all piezometers, so we matched intervals of heavy rainfall at the throughfall gauges to the intervals of rapid increase in water level in the piezometers (> 0.3 mm / h). We treated each contiguous interval of rapidly increasing head as a storm, then searched the throughfall time series for the corresponding record of that storm, considering that it might be slightly offset in time. Usually there was only one heavy rain that overlapped with the increasing head interval; in rare cases, there were two. In those cases we chose the storm with the higher total depth, assuming that it would be more likely to cause the rapid increase in water level. If the time offset for onset of the storm differed by more than 1 h, the candidate storm was discarded.

We then assembled the water level response to rain storms into a single master rising curve using the same least-squares method we applied for the recession analysis. Because the water level rose much faster during a heavy storm than it receded after the storm, we assumed that the total storm depth was a good approximation for the increase ΔS in water storage during the storm that drove the rise $\Delta \zeta$ in the water level. Our goal in this analysis was to minimize the least-squared difference in storage S corresponding to each water level ζ . Each storm was represented by the initial and final water level (ζ_o, ζ_*) and by an initial, unknown storage S_o and a final storage S_* increased from initial storage by the total storm depth P ($S_* = S_o + P$). These line segments were then interpolated at 1 mm increments of head and aligned by least squares in the same way as the recessions in the recession analysis. Again [and contrary to *Cobb et al.*, 2017], we set up the system

of equations so that the arbitrary reference storage was zero at a water level of zero (water table at bottoms of hollows) so that additional, lower water level data would not affect the horizontal position of the master rising curve.

2.5 Hydrologic parameterization

We used the master rising and recession curves to estimate peat hydraulic parameters (Figure 4). Because tropical peat deposits are thousands of times broader than they are thick [Anderson, 1964; Hooijer, 2005], we interpreted water-table behavior using Boussinesq's equation for approximately horizontal flow: a change in storage (differential change in water table H times specific yield $S_y(\zeta)$) is driven by precipitation P , evapotranspiration ET , and divergence of groundwater flow $\nabla \cdot (T(\zeta)\nabla H)$

$$S_y(\zeta) \frac{\partial H}{\partial t} = P - ET + \nabla \cdot [T(\zeta)\nabla H],$$

where both the specific yield $S_y(\zeta)$ and transmissivity $T(\zeta)$ are nonlinear functions of water level ζ and more generally could vary with location.

As shown in Cobb *et al.* [2017], the similar water level response across piezometers (Figure 3b) can be used to simplify Boussinesq's equation further. First, we express the water-table elevation H as the sum of the peat surface elevation p and the water level ζ

$$S_y \frac{\partial(p + \zeta)}{\partial t} = P - ET + \nabla \cdot [T\nabla(p + \zeta)].$$

The peat surface elevation p is practically constant on the time scale of typical hydrologic applications ($\partial p / \partial t \approx 0$) and the water level ζ is approximately spatially uniform (Figure 3b; $\nabla \zeta \approx 0$) yielding a simpler equation for the dynamics of the water level ζ

$$S_y(\zeta) \frac{d\zeta}{dt} = P - ET + \nabla \cdot [T(\zeta)\nabla p]. \quad (5)$$

We applied this water level dynamics equation (5) to interpret the master rising and recession curves and estimate the specific yield and transmissivity functions $S_y(\zeta)$, $T(\zeta)$.

Under very heavy rain the groundwater divergence term in equation (5) becomes negligible relative to precipitation $\nabla \cdot (T\nabla p) \ll P$, yielding the approximation

$$S_y(\zeta) \frac{d\zeta}{dt} \approx R.$$

This approximation is the essence of the rain-to-rise approach first applied by White [1932].

The total rain depth P required to raise the water level from an initial level ζ_o to a final

level ζ_* is the integral of specific yield between those positions ζ_o, ζ_* in the soil profile

$$P = \int_{\zeta=\zeta_o}^{\zeta_*} S_y(\zeta) d\zeta. \quad (6)$$

Therefore the inverse slope of the master rising curve provides an estimate of the specific yield function (Figure 4c).

We further simplify the equation for water level dynamics by making use of the similarity in recessions across piezometers and interstorms, under the hypothesis that peat hydraulic properties can be described by two functions, the specific yield as a function of water level $S_y(\zeta)$ and the transmissivity as a function of water level $T(\zeta)$ [Cobb *et al.*, 2017].

If so, there is no spatial gradient in the transmissivity $\nabla T = 0$ because there is no gradient in the water level $\nabla \zeta = 0$, and water level dynamics are described by

$$S_y(\zeta) \frac{d\zeta}{dt} = P - ET + T(\zeta) \nabla^2 p. \quad (7)$$

The recession of the water level during interstorms is driven by the divergence of groundwater flow $T \nabla^2 p$ and evapotranspiration ET

$$S_y \frac{d\zeta}{dt} = -ET + T \nabla^2 p.$$

Once multiple recessions have been superimposed in the master recession curve, day and night from the recessions are intermixed depending on the time at which each interstorm began, and the diurnal fluctuations in recession from evapotranspiration become obscure (Figure 4d). Therefore, in analyzing the master recession curve we take evapotranspiration as constant and equal to its average through the diurnal cycle \overline{ET} to obtain a simplified differential equation without rain which, in its integral form,

$$t = \int \frac{S_y(\zeta)}{-\overline{ET} + T(\zeta) \nabla^2 p} d\zeta + \text{constant} \quad (8)$$

is equivalent to the master recession curve (Figure 4d) turned on its side [Cobb *et al.*, 2017].

We estimated the hydraulic conductivity and specific yield profiles from the master rising curve and master recession curves after Cobb *et al.* [2017], with the minor change that the lowest knot in the hydraulic conductivity profile was moved from a level of -11.2 cm to the bottom of the recession curve at -29.2 cm. This change allowed conductivity to continue to decrease in the soil profile down to the lowest recorded water levels and resulting in a better overall fit. We made an initial estimate of the specific yield function

$S_y(\zeta)$ (represented as a cubic spline) by fitting the rising curve (water level vs. cumulative rainfall depth $\zeta(P)$, equation 6) using nonlinear least-squares (Levenberg-Marquardt). At low water tables, the water level was nearly constant at night but decreased linearly during the day (Figure 3d), so we estimated evapotranspiration (ET) from the daytime decrease in water table and specific yield obtained from the master rising curve. We then estimated the transmissivity function $T(\zeta)$ (represented as the piecewise-linear logarithm of its derivative, hydraulic conductivity) by fitting the recession curve (water level ζ vs. time since rain, equation 8) with our initial estimate of the specific yield function $S_y(\zeta)$. The Laplacian $\nabla^2 p$ was obtained from topographic data as described above (“Topographic analysis”).

We then refined our estimates of the specific yield and transmissivity functions $S_y(\zeta)$, $T(\zeta)$ by simultaneously fitting the rising and recession curves by nonlinear least squares using the PEST Model-Independent Parameter Estimation and Uncertainty Analysis package [Doherty, 2010]. Performing this joint fitting step yields a more accurate estimate of the specific yield and transmissivity because the water level decreases more slowly during interstorms than it increases during storms (see Discussion). We simulated rising and recession curves using their respective definitions (equations 6 and 8) with an integrating solver [Hindmarsh et al., 2005]. The objective function was the sum of squared differences between observed and simulated dynamic storage (master rising curve) and elapsed time (master recession curve) at each 1 mm increment of water level from -29.1 cm through 14.8 cm. All residuals (440 residuals for master rising curve, 440 residuals for master recession curve) were weighted equally in the fit. Conductivity was log-transformed during optimization. The correlation among parameters and linearized confidence intervals in the neighborhood of the solution were obtained from PEST outputs.

2.6 Water balance calculation

We used the rising curve and our estimate of evapotranspiration from analysis of recession curves to calculate an estimated water budget for our site, after Hooijer [2005]. We calculated the change in storage over the year by converting the initial and final water levels ζ to storage S using the rising curve, and obtained total evapotranspiration over the year as the product of the average daily evapotranspiration \overline{ET} and the total duration of the year.

2.7 Simulating discharge with a scalar model

Because the rise in the water level during storms and its recession during interstorms are approximately functions of the water level alone, we explored a simple nonlinear bucket model for the hillslope hydrology of natural tropical peatlands based on the master curves (Figure 5). The essence of this model is that rain causes an increase in water storage in the hillslope, described by the master rising curve, whereafter the stored water drains out of the peatland at a rate that depends nonlinearly on the amount of water remaining. The approximations used in the scalar model are that (1) the water table is near the surface, near-surface hydraulic conductivity is very high, infiltration is very fast and infiltration capacity is not limiting; and (2) there is no non-Darcian overland or channel flow within a hydrologic response unit. Instead, as the water table rises within the peat, flow to bounding channels increases greatly because of an exponential increase in transmissivity. These assumptions eliminate the surface water, routing, and soil moisture stores found in typical explicit-soil-moisture-accounting (ESMA) models [Figure 5; *Beven, 2012*], but add a strongly nonlinear storage-vs-discharge function because of the curved transmissivity profile derived from the master recession curve analysis (Figure 4f).

The master curves themselves provide an adequate system for simulating the hydrologic response of the peatland without further parameterization, because they describe how the water level goes up in an arbitrary storm and how it declines during interstorms (Figure 6a–d). To obtain discharge, however, the effect of evapotranspiration needs to be separated out. The discharge term is simply the groundwater divergence term $T\nabla^2 p$ in the ordinary differential equation. This represents also the discharge to the bounding stream or river, within the approximation of the model. Thus, the hillslope discharge Q is simply the transmissivity times the (uniform) Laplacian of surface elevation

$$Q = -T(\zeta) \nabla^2 p. \quad (9)$$

We used the specific yield $S_y(\zeta)$ and transmissivity $T(\zeta)$ functions and evapotranspiration from our analysis of the rising and recession curves with the peat surface Laplacian $\nabla^2 p$ from our topographic analysis to simulate the rainfall-runoff response of our peatland hillslope. In tropical peatlands, storage S is simply obtainable from water level ζ . However, in most other catchments, discharge Q can be monitored easily but storage S cannot. Therefore, the convention in most scalar catchment models is to represent the hydraulic state of the catchment via the discharge Q . For example, the “recession plot” of *Kirch-*

ner [2009] [after *Brutsaert and Nieber*, 1977] regresses the rate of decrease in discharge $-dQ/dt$, or “recession rate” against the discharge Q . For comparison with the literature, we calculated the recession rate $-dQ/dt$ from the discharge (equation 9) using the chain rule

$$-\frac{dQ}{dt} = -\frac{dT}{d\zeta} \frac{ET + Q}{S_y} \nabla^2 p.$$

Another quantity that is frequently used in scalar catchment models is the recession time “constant”, or differential change in storage from a change in discharge dS/dQ . Again applying the chain rule, we computed the recession time “constant” as

$$\tau = \left[\frac{dQ}{dS} \right]^{-1} = \left[\frac{-\nabla^2 p}{S_y} \frac{dT}{d\zeta} \right]^{-1}. \quad (10)$$

Noting the strong effect of catchment state / antecedent moisture on the recession time “constant,” we also explored the effect of antecedent moisture on the simulated discharge response of the catchment to different design storms. We used the simplified ODE for water level (equation 7) to simulate the response of the water level and discharge to rain storms of 10 mm / h or 20 mm / h and total depth 20, 40, and 60 mm, and with dynamic storage prior to the storm of 0 through 50 mm at 5 mm intervals ($\{0, 5, 10, \dots, 50\}$ mm). Discharge during and after the storm was computed from equation (9).

2.8 Effects of rainfall intermittency on discharge

Because of the projected increase in rainfall variability in many tropical peatland areas [*Huang et al.*, 2013; *Kang et al.*, 2019], we explored the effects of increased rainfall intermittency on peak discharge. We repeatedly simulated three-year intervals of rain storms as a Poisson process with exponentially distributed depths in each storm, to find the average 95th percentile of peak discharge over 3-year intervals for a range of mean interstorm arrival times. We first generated a sequence of 16,000 storms as a Poisson process with unit mean interstorm arrival time and depth. For each specified mean precipitation and interstorm arrival time, we scaled the storm times and depths to match the desired means, and then simulated the response of the water level and discharge to the storm time series using the parameterized functions and peat surface Laplacian obtained from our field site as described above. We determined the end of a three-Gregorian-year time interval, after a 2000 storm spin-up period, by bisection, and determined the 95th percentile of peak discharge on that 3-year interval by sorting peak water levels followed by linear interpolation (peak water levels could be obtained easily because they always coincide with a storm

impulse). The same procedure was repeated 30 times for each combination of mean interstorm arrival time and mean storm depth with different random series of storms, and the mean and standard error of discharge across all 30 of the 3-year time intervals was recorded. To verify that the spin-up period of 2000 storms was long enough that the water level prior to spin-up had a small effect on these quantiles, we replicated these runs with initial water levels of -230 mm, 30 mm, and 98 mm (approximately 5th, 50th, and 95th percentiles of recorded water level) and compared the 95th percentile of 3-year discharge peaks under these different initial conditions.

3 Results

3.1 Topographic analysis

Our straight-line fit to the integrated-gradient vs. contributing area curve in the region of uniform water-table behavior gave an average peat surface Laplacian $\overline{\nabla^2 p}$ in the region of the piezometers of $-2.36 \times 10^{-3} \text{ km}^{-1}$, corresponding to a TWI of about 13 log m (Figures 1,2).

3.2 Water-table rise and recession analysis

The water-table response was very similar among the four piezometers in the area of approximately uniform Laplacian (Figures 2,3). The recession of the water table from a given initial level was also very similar across interstorms (Figure 3b), resulting in a well-defined master recession curve (Figure 3f). The master recession curve indicates that the water table would take about 25 days to recede from its highest extent (15 cm above the bottoms of hollows) to its lowest extent (30 cm below the bottoms of hollows).

The rise of the water table in response to rain had similar behavior across piezometers and across storms as well (Figure 3b) and could be assembled into a master rising curve, although the curve is somewhat more jagged than the master recession curve (Figure 4c). The master rising curve suggests that the range of water-table fluctuations, from 30 cm below the bottoms of hollows to 17 cm above the bottoms of hollows, corresponds to a range of 14 cm of fluctuations in dynamic storage.

3.3 Hydrologic parameterization

Our functions for peat specific yield vs. water level $S_y(\zeta)$ and transmissivity vs. water level $T(\zeta)$, parameterized from the master rising and recession curves, are shown in Figure 4. Analysis of the rising and recession curves indicates that the specific yield is about 0.69 high in the soil profile (16.8 cm above the bottoms of hollows; Figure 4e) but drops below 0.2 deeper in the soil profile (6.2 cm below the bottoms of hollows). The transmissivity increases roughly exponentially as the water level rises, going from less than $10 \text{ m}^{-2} \text{ d}^{-1}$ when the water table is below the bottoms of hollows (below -16.8 cm) to over $10^5 \text{ m}^{-2} \text{ d}^{-1}$ when the water table rises to 15 cm above the bottoms of hollows. The transmissivity profile implies a range of hydraulic conductivity (derivative of transmissivity) from $6.0 \times 10^{-5} \text{ m s}^{-1}$ at 29.1 cm below the bottoms of hollows to 73 m s^{-1} at 16.8 cm above the bottoms of hollows, with an inflection near the bottoms of hollows, where the conductivity was $1.5 \times 10^{-2} \text{ m s}^{-1}$.

The correlations between specific yield and conductivity parameters were fairly weak (0.23 or less), and linearized 95% confidence ranges were small for all the parameters (Figure S1). The strongest of the correlations between the specific yield and conductivity knots occurred in the middle of the profile, near a water level of zero. This corresponds to a range where discharge is relatively small but evapotranspiration is not large enough to strongly distinguish between the effects of conductivity and specific yield in the master recession curve. The correlations between log-conductivities at adjacent knots were stronger, because the conductivity on a segment of the conductivity profile is affected by the knot on either side of the segment; correlations between specific yield knots extended further because a single span of a cubic spline is affected by the 4 neighboring control points.

Analysis of the recession of the water table during the day and at night gave an estimate of 2.25 mm / d evapotranspiration (ET). Evapotranspiration estimated from water-table movements represents loss from the connected pore water and surface water, not the total evapotranspiration from the forest. Total evapotranspiration from the forest also includes water intercepted by the canopy and leaf litter layer, and is probably considerably higher (Discussion).

3.4 Water balance calculation

The increase in stored water in the peatland over the year, or recharge, was about 0.5 mm: the water table was 1.8 mm higher at the end of the data interval (2013-02-18) than at the beginning (2012-02-07), and the specific yield in that water level range (4.35 cm to 4.53 cm) averages 0.29 (Figure 4e). Our evapotranspiration estimate (“Hydrologic parameterization”, above) implies that 85 cm of the 165 cm of throughfall that reached the peat at our site was lost as evapotranspiration from the peat in 2012. In our annual budget, discharge is the difference between net precipitation and change in storage (recharge; Figure 5). Because of the small (0.5 mm) recharge term, water lost as discharge via divergence of groundwater flow was approximately equal to net precipitation, or 80 cm.

3.5 Simulating discharge with a scalar model

Calculations of peat hillslope discharge based on hydrologic parameterization (Figure 6) showed a very strong effect of initial water level (Figures 7,8). Discharge is an approximately exponential function of storage (Figure 7a), and therefore the rate of change in calculated discharge (recession) declined rapidly at lower discharge (Figure 7b). This strong dependence of the recession on the hillslope hydraulic state resulted in a large range of apparent recession time “constants” (e-folding time of decrease in discharge during recession), from over 70 d at the lowest water levels to less than 2 h at the highest (Figure 8a).

The exponentially greater discharges at higher water tables caused the shape of the calculated hillslope discharge hydrograph and the peak discharge for a given design storm to change greatly depending on discharge at the start of the storm (Figure 8b). The nonlinearity of the storm response resulted in a strong effect of antecedent moisture expressed as pre-event discharge or water level on the peak discharge. If the initial water level was set near the bottoms of hollows, peak discharge, while many times larger than initial discharge, was still very small (Figure 8c,d). However, at higher water tables (more than 10 cm above the bottoms of the hollows), calculated peak discharge began to approach the rainfall intensity itself during the design storms of greatest depth (6 cm; Figure 8c,d).

3.6 Effects of rainfall intermittency on discharge

Peak simulated discharge (mean 95th percentile of discharge peaks on 3-year intervals) increased strongly and nonlinearly with net rainfall and mean interstorm arrival time in

our simulations of discharge response to Poisson-process storms with exponentially distributed depths (Figure 9). The 95th percentile of discharge peaks simulated on 3-year intervals was 0.02 mm / h at the lowest net rainfall intensity (0.2 mm / d) and shortest mean interstorm arrival time (2.4 h), and increased to 11.8 mm / h at the highest net rainfall intensity (7 mm / d) and longest mean interstorm arrival time (1.5 d). Pre-spin-up water level had a small effect on peak discharge: the largest effect was a difference in peak discharge of about 3.2% with a pre-spin-up water level of -23 cm versus 9.8 cm for the lowest mean net precipitation (0.2 mm / d) and shortest mean interstorm arrival time (2.4 h). For all other values of mean net precipitation, the effect of pre-spin-up water level was less than $10^{-5}\%$.

4 Discussion

A scalar model attempts to summarize the state of a hydrologic system with a single number, such as total water storage or the discharge from a catchment. In evaluating the applicability of a scalar model, the key question is: given an initial state as represented by the scalar, is the response of the hydrologic system across events approximately the same? Empirical and theoretical work in hillslope hydrology has shown that in general the answer to this question is no: discharge may progress differently, and respond differently to rainfall, depending on the distribution of water within a hillslope, not just the total amount [Hewlett and Nutter, 1970; Freeze, 1972; Dunne, 1978].

Observations in tropical peatlands, though, suggest that the response of the water level to rainfall and dry intervals is remarkably predictable. First, the position of the water table relative to the peat surface is strikingly similar at different locations in the peatland [Figure 3b; Hooijer, 2005], indicating that gradients in the peatland water table remain almost constant with time. Second, the response of the water level to rain and its recession after rain is similar across events (Figure 3,4). To the extent that a scalar approximation is descriptive, the single-storm water-table vs. rain depth and single-interstorm water-table vs. time curves will fall on well-defined aggregate curves for rise and recession (Figure 4). If the scalar approximation to water table were poor, this would be apparent as individual curves that diverge, indicating that on different occasions, the hydraulic response was different [cf. discharge hydrographs in Nathan and McMahon, 1990]. We conclude that a scalar model can provide a good approximation to tropical peatland water-table behavior, at least in natural peatlands (Figure 4).

What is it about tropical peatlands that allows a simple nonlinear bucket model to do a relatively good job of capturing their hydrology? Three factors contribute to the accuracy of the scalar approximation in tropical peatlands: (1) a uniformly thin vadose zone; (2) the nearly uniform Laplacian of the peat surface elevation; and (3) the persistent microtopography of the peat surface. The vadose zone is uniformly thin because the water table remains within tens of centimeters of the peat surface over the entire peatland. Because the vadose zone is thin and nearly saturated, rain easily infiltrates to the water table within the time span of a storm, and vadose zone soil moisture is insignificant to water balance calculations. The thin vadose zone and fast water table response removes a major factor that contributes to the complexity of general hillslope response, in which vadose zone water can continue to contribute to outflow over days [Hewlett and Nutter, 1970] and the slow redistribution of vadose zone water leads to a strong history-dependence in storm response [Dunne and Black, 1970; Freeze, 1972].

A second factor leading to scalar behavior in tropical peatlands is the special shape of the peat surface and the groundwater mound. Because of the nearly uniform Laplacian of the peat surface, during rain storms the water table rises through the vadose zone approximately synchronously across the hillslope. The synchronized saturation of the vadose zone removes a second major factor that contributes to complex hillslope response in classical studies, in which saturation occurs from the bottom to the top of the hillslope [Dunne, 1978]. In those studies, differential saturation near the bottom of the hillslope and slow redistribution of water result in large spatial differences in unsaturated conductivity through the hillslope depending on the local distribution of water in the vadose zone [Hewlett and Nutter, 1970; Dunne, 1978]. In natural tropical peat hillslopes, the vadose zone instead has a similar thickness throughout the peatland [Figure 3; Hooijer, 2005], and is likely to have a nearly hydrostatic moisture distribution, minimizing spatial gradients in the conductivity of the surface layer where most flow occurs.

We believe that a third factor that leads to similar water table response across storms in natural peatlands is the persistent microtopography of tropical peatlands and the absence of ephemeral streams [Ritzema et al., 2014; Lampela et al., 2016]. In other settings, the soil surface tends to a relatively flat morphology dissected by streams because of settlement and erosion of granular soils. In tropical peatlands, the structures created by trees and woody debris resist these processes, creating a persistent non-channel morphology in which the water table can rise above the surface in hollows without giving rise to tur-

bulent overland flow. Observation of the forest floor at our site, as well as in Kalimantan [Lampela *et al.*, 2016], show that hollows are not connected; to pass from one hollow to the next, water is forced to flow through porous media retained by buttresses, woody rhizomes of giant herbs, and coarse woody debris. A 200 m survey of the peat surface at our site showed that the tops of amorphous peat hummocks rise to about 20 cm above the reference water level [Cobb *et al.*, 2017], and woody structures that block flow rise more than a meter above the peat surface. Over nine years of field work, including during heavy storms in very wet conditions, we have observed no overland sheet or channel flow.

The three factors described above—the thin vadose zone, uniform Laplacian of the peat surface elevation, and persistent microtopography—lead to approximately uniform water table fluctuations in tropical peatlands. A major benefit of the uniform fluctuation of the water table for hydrologic analysis is that the effects of topography and of the hydraulics of the peat on the recession of the water level can be neatly separated. The approximations of uniform water table fluctuations and uniform hydraulic properties lead to the separability of transmissivity and topography in the Boussinesq equation, so that they become two separate multiplicative factors $T\nabla^2 p$ (equation 7) instead of being entangled within the groundwater divergence term $\nabla \cdot (T\nabla H)$ (equation 5). Because of this separability, after calculating a single metric of landscape topography—the Laplacian of the peat surface elevation, or the TWI (Figure 1,2)—the conductivity and specific yield profiles can be estimated based on fluctuations of the water table (Figure 4).

The separability of peat hydraulics from topography and forcing allows estimation of the conductivity of the surface layer where most flow occurs, which is very hard to measure by other methods (Figure 4). Standard piezometer tests cannot be used to measure the permeability of the surface layer because of the very rapid response of the water table [Takahashi and Yonetani, 1997; Baird *et al.*, 2017]; the water level inside the test piezometer equilibrates almost instantly with the water table nearby. Similar difficulties have been reported in measurements of peat conductivity in the upper soil profile in higher-latitude peats [Boelter, 1965; Bromley *et al.*, 2004; Surridge *et al.*, 2005]. Some studies of temperate peats have found good agreement between piezometer test and laboratory measurements of hydraulic conductivity [Surridge *et al.*, 2005]. However, the complex of amorphous peat, roots, rhizomes, and coarse woody debris in the surface layer of natural tropical peats would make representative sampling and the derivation of effective bulk conductivities from laboratory measurements extremely challenging. Deeper peat too may

contain large pores: peat cores often include voids tens of centimeters long [Dommain *et al.*, 2015], and we have found fish approximately 10 cm long in freshly formed pools kilometers from the nearest river, suggesting a network of macropores with diameters on the scale of centimeters, analogous to the pipes described in temperate peatlands [reviewed in Holden, 2005]. Pump tests have been applied to measure the hydraulic conductivity of peat at moderate depths in higher latitude peatlands [Bromley *et al.*, 2004], but applying pump tests to measure the conductivity of the surface layer in tropical peat is impractical. The master curve approach, in contrast, effectively averages over a large horizontal scale, avoiding the sampling and averaging issues that occur using piezometer tests [Binley *et al.*, 1989; Bromley *et al.*, 2004], and requiring only measurements of water table fluctuations and throughfall.

The conductivity and specific yield profiles obtained from the scalar approximation can be applied in other peatlands with similar vegetation and peat structure. The parameters of many scalar models describe the combined effects of hydraulics, topography and evapotranspiration on the decline in the water table, recession of discharge or decrease in soil moisture after rain [e.g., Rodriguez-Iturbe *et al.*, 1999; Field *et al.*, 2004; Kirchner, 2009; Kurnianto *et al.*, 2015; Koster *et al.*, 2017]. Simulation based on such parameters is analogous to simulation using the master curves alone (Methods 2.7), and parameterization will be applicable only in other catchments where hydraulics, topography and evapotranspiration are all similar. But by analyzing the master curves using topography to obtain conductivity and specific yield profiles, we obtain hydraulic properties that could be applied in other catchments where vegetation and peat are similar but topography and forcing are different. In addition, initial estimates for hydraulic parameters in higher-dimensional models [e.g., DigiBog; Baird *et al.*, 2012] can also be obtained from the conductivity and specific yield profiles provided by the scalar approach.

4.1 Hydraulic conductivity profile

The conductivity values we obtain from the scalar approach in the deeper part of the profile are lower than estimates of conductivity at similar depths from two studies using piezometer tests in Peru and Panama [Kelly *et al.*, 2014; Baird *et al.*, 2017]. We estimate a conductivity of $6.0 \times 10^{-5} \text{ m s}^{-1}$ (5.2 m d^{-1}) at a depth of 29.1 cm below the bottoms of hollows. Kelly *et al.* [2014], in San Jorge ombrotrophic domed peatland in Peru, measured a median conductivity of $4.64 \times 10^{-3} \text{ m s}^{-1}$ (401 m d^{-1}) at 50 cm depth. Baird *et al.*

[2017] measured an arithmetic mean conductivity of $5.46 \times 10^{-3} \text{ m s}^{-1}$ (472 m d^{-1}) at a depth of 0.55–0.65 m in hardwood peat forest in Panama. *Takahashi and Yonetani* [1997] measured conductivity of peat with slug tests at a site near Palangka Raya, Central Kalimantan, Indonesia, but found that the conductivity was too high to measure at a depth of less than 1 m (more than 10^{-4} m s^{-1} , or 8.64 m / d). The higher conductivities at around –50 cm found in these studies using piezometer tests could indicate that the effective average conductivity is closer to the harmonic or geometric mean rather than the arithmetic means reported in the literature, or that slug test results are influenced by higher conductivity above the depth of the well screen. Our estimates of conductivity higher in the soil profile — $1.5 \times 10^{-2} \text{ m s}^{-1}$ ($1.3 \times 10^3 \text{ m d}^{-1}$) at the bottoms of hollows, and 73 m s^{-1} ($6.3 \times 10^6 \text{ m d}^{-1}$) at 16.8 cm above the bottoms of hollows — have no counterparts in the tropical peat literature because effective conductivity at this depth cannot be measured with piezometer tests. Estimates of hydraulic conductivity in temperate peatlands span $0.7 \times 10^{-5} \text{ m s}^{-1}$ to $1.3 \times 10^{-2} \text{ m s}^{-1}$ ($0.6\text{--}1.1 \times 10^3 \text{ m d}^{-1}$) [reviewed in *Rezanezhad et al.*, 2016], a similar range to our subsurface estimates, and have also often revealed strong gradients with depth [differences up to 5–6 orders of magnitude from surface to 50 cm depth; *Boelter*, 1965; *Hoag and Price*, 1995; *Baird et al.*, 2016].

4.2 Specific yield profile

Our initial estimate of the specific yield profile $S_y(\zeta)$ was based on fitting the master rising curve alone, and thus effectively determined the specific yield as the derivative of the net depth of rainfall per rise in water table during periods when rainfall and infiltration were much faster than divergence of horizontal flow. This approach, derived from work by *White* [1932], has been applied in the Everglades of North America [*Dolan et al.*, 1984], and in tropical and temperate peatlands [*Hooijer*, 2005; *Dettmann and Bechtold*, 2016] and is sometimes termed the “rain-to-rise ratio” approach, or the “WTF method” [water table fluctuation; *Healy and Cook*, 2002].

After this initial fit to the rising curve, we further adjusted the specific yield profile in a joint fit to the master rising and recession curves. Because the fit to the rising curve had already been optimized, it could not be improved by further adjusting the specific yield during the joint fit. However, the joint fit resulted in a much better fit of the recession curve while having only a slight effect on the rising curve. The reason for this lies in the flattening and then steepening of the recession curve at a water level of about –3 cm (be-

tween regions B and C in Figure 4d). The rising curve in this range of water levels seems to have a constant slope, suggesting a constant specific yield. However, if specific yield were constant, the increase in recession rate at this water level could only be explained by a (non-physical) negative conductivity. A simple explanation is that this inflection arises from a vertical gradient in specific yield in this part of the soil profile that is not apparent in the rising curve. The rising curve is assembled from straight line segments connecting the water level before and after heavy rain storms, in which the water table may rise by 8 cm or more, so it may not capture every change in slope arising from a gradient in specific yield. If we had fixed the specific yield as constant in this range after fitting the rising curve, the optimization would not have been able to find a solution with good fits to both the rising and recession curves: parameterizations without the inflection around 0 cm could not reproduce the slower decline in the water table at that water level (zone B in Figure 4d).

Our estimated specific yield profile (Figure 4e) has similar characteristics to specific yield profiles reported from both tropical and temperate peatlands. *Hooijer* [2005] used the rain-to-rise approach to estimate a specific yield of 0.71 for the top 10 cm of the peat profile and 0.29 for greater depths, similar to the maximum of 0.68 we estimated at 16.8 cm and approximately 0.29 in the range of 0 to 5 cm above the bottoms of hollows, although our estimate suggests that the specific yield declines further lower in the soil profile (Figure 4e). We believe that the inflection between regions B and C reflects a genuine feature of the peat and vegetation at these sites, perhaps caused by a “void layer” that is sheltered from direct litter fall by the skeleton of buttress roots above the level of the bottoms of hollows. Intriguingly, a similar local maximum near the peat surface has been observed in profiles of external porosity in the former USSR, there attributed to a “roof” of *Sphagnum* moss side branches on a less dense layer of vertical stalks [*Romanov*, 1968; *Ivanov*, 1981].

4.3 Interpretation of the master curves

The recession of the water table during interstorms is steep and apparently exponential at the highest water levels, more than about 3.4 cm above the bottoms of local depressions in the peat surface (hollows), when it is dominated by divergence of groundwater flow (regime A in Figure 4d). Although the specific yield is highest in this portion of the profile (Figure 4e), it is more than compensated by the much higher transmissivity at these water levels (Figure 4f), so the water table falls very fast. In the next range of water lev-

els, near the bottoms of hollows (regime B; -2.2 – 3.4 cm), the recession is the slowest. Although runoff is higher at these water levels than it is lower in the soil profile (because of higher transmissivity; Figure 4f), the higher specific yield at this range of water levels (Figure 4e) causes the water table to decline more slowly. When the water table is lower than the critical level of 2.2 cm below hollows, its recession becomes approximately linear with time, with a distinct diurnal fluctuation from evapotranspiration (regime C in Figure 4d). At our site, the water table declines faster below this critical level (regime C) than it does higher in the soil profile because of the lower specific yield.

4.4 Evapotranspiration

White [1932] used diurnal fluctuations in water-table recession in combination with specific yield measurements to estimate evapotranspiration, much as we did, and a similar approach has been applied in other studies of wetland hydrology [Dolan *et al.*, 1984; Hooijer, 2005]. Our evapotranspiration estimate (2.25 mm / d; “Hydrologic parameterization”, above) implies that 848 mm of the 1647 mm of throughfall that reached the peat at our site was lost as evapotranspiration from the peat in 2012. Using a similar approach, Hooijer [2005] estimated evapotranspiration of 2.94 mm / d at a site in Sarawak, also in north-west Borneo. Our estimate represents water lost from the peat, and not the total evapotranspiration to the atmosphere, which would also include rain that is intercepted by the canopy, understory or litter and evaporates without reaching the water table. Some error is also likely because of the spatial heterogeneity of throughfall. Because precipitation from convective storms in the region is highly localized [Bidin and Chappell, 2006; Kang *et al.*, 2019], it is difficult to infer anything further from these values without direct measurements of above-canopy precipitation.

4.5 Applications

4.5.1 Water table forecasts

The scalar approach in tropical peatlands enables predictions of drying trajectories and water table distributions with limited instrumentation. Because of the approximately uniform fluctuations of the water table, a relatively small number of water table time series can be collected to represent a large area. Once master rising and recession curves have been constructed, they can be used for forward simulation of average water tables given

precipitation forecasts. Peatland flammability increases as peat dries [Usup *et al.*, 2004], so being able to predict how long it will take the water table to reach a critical depth is useful in predicting vulnerability to fires. Also, as subsidence of peat from organic decomposition is proportional to the time-averaged water table depth, scalar simulations allow prediction of how subsidence will proceed in a peatland following a decrease in rainfall amount or frequency. The ability to extract conductivity and specific yield profiles from master curves makes it possible to then construct similar projections in other peatlands with similar vegetation but different topography.

4.5.2 Soil moisture forecasts

Uniform water level fluctuations suggests that vadose zone soil moisture is also relatively uniform across a peatland, making the “loss function” approach to modeling soil moisture dynamics viable [Koster *et al.*, 2017; Akbar *et al.*, 2018]. Particularly in combination with satellite measurements of soil moisture [Dadap *et al.*, 2019], scalar models could be used in a predictor-corrector framework to forecast peatland fire vulnerability [analogous to drought code prediction in Shawki *et al.*, 2017]. A more detailed model and thorough verification are preferable where measurements are available to constrain model parameters and boundary conditions; however, the scalar approach can provide preliminary predictions until such data are available.

4.5.3 Modeling runoff generation

The scalar approach also generates testable hypotheses about discharge from tropical peatlands. By multiplying the rate of decline in the master recession curve by the specific yield derived from the rising and recession curves, the water level master curves becomes a discharge function (Figure 4f) describing hillslope runoff generation. Using this discharge function and the cumulative distribution of the water level in the peatland (Figure 4h), we can estimate the contributions of the different regimes of the recession curve to discharge. The peatland spends about 48% of its time with the water level in the highest range (A), but the high discharge at those water levels accounts for 97.8% of the runoff in this natural peatland. Regime B accounts for 16% of our observations, and 1.6% of the discharge; and regime C accounts for 36% of our measurements, but only 0.6% of discharge. For comparison, using runoff troughs, Holden [2005] observed that 99% of the

runoff from a blanket peatland hillslope in Upper Wharfedale, UK occurred from the top 20 cm of the soil profile, 95% from the top 8 cm, and 74% from the top 1 cm.

In our model, there is a one-to-one relationship between dynamic storage S and discharge from the hillslope $Q = T\nabla^2 p$ because transmissivity is a function of the (uniform) water level ζ , which is convertible to dynamic storage via the hillslope specific yield. Assuming the peat is underlain by an aquiclude, or the low-permeability deep peat itself forms an aquiclude, throughfall must be lost either to the bounding streams or as evapotranspiration, and the unsaturated zone is too thin to contribute much to an intermediate- or long-term water budget. Our approach may not capture the timing and magnitude of peaks in discharge from the peatland [cf. *Dunne*, 1978, p. 289], and these peaks are important for design hydrology in tropical peatland catchments. However, our approach accounts for all throughfall, and therefore should capture most runoff generation in the peatland.

When viewed in this way, our scalar model closely resembles the scalar catchment models described by *Lambert* [1969, 1972] and popularized by *Brutsaert and Nieber* [1977] in which catchment discharge Q is assumed to have a one-to-one relationship with catchment storage S . As a special case, *Brutsaert and Nieber* [1977] examined catchments in which the recession is related to the discharge via a power law $dQ/dt = aQ^b$. If the exponent $b = 2$, discharge is an exponential function of storage when evapotranspiration is negligible [*Jepsen et al.*, 2016]. Our calculated discharge recession curves closely resemble those observed by practitioners of these methods, such as *Kirchner* [2009] and *Jepsen et al.* [2016], because of the approximately exponential relationship between discharge and storage we derived from the master rising and recession curves. Our calculated recession vs. discharge curve deviates from a straight line on a log-log-plot ($dQ/dt = aQ^b$) because of evapotranspiration, as discussed by *Jepsen et al.* [2016]. Interestingly, the Dee and Plynlimon (Wye and Severn) catchments studied by *Lambert* [1969, 1972] and by *Kirchner* [2009] both include peat headlands.

We explored the implications of our model for runoff generation in tropical peatlands by simulating the response of peatland discharge to design storms (Figures 7–9). Simple as it is, a scalar model captures an important aspect of hillslope discharge in tropical peatlands: the strong dependency of the discharge profile during a storm on antecedent moisture (Figure 8). We evaluated discharge after storms of a distribution of depths and durations given different antecedent moisture status, represented by different initial dynamic storage

S (Figure 8). Wetlands have been described as being like sponges [Acreman and Holden, 2013, provide a history of this analogy], and tropical peatlands may absorb rain storms with little increase in discharge during dry times. However, as the water table rises, the behavior of the peatland becomes increasingly flashy, manifested as a dramatic decrease in the recession time “constant,” or e-folding time of the decay in discharge [Kirchner, 2009], at high water levels (Figure 8a). Whether a peatland behaves like a sponge or a rock in response to a design storm depends on whether the initial storage is low or high (Figure 8). In this sense, scalar catchment models contrast with unit hydrograph theory, which assumes that a storm has the same effect on stream flow regardless of the antecedent moisture [Figure 8b; Dooge, 1959; Kirchner, 2009].

Whatever the antecedent moisture, the scalar approximation predicts that peak runoff generation will occur at or before the end of rainstorms (Figure 8b). This pattern is consistent with what is known about raised bog headwater catchments in temperate zones [Ingram, 1983], but differs from late peaks in discharge that can occur in hillslopes dominated by slow vadose zone dynamics [Hewlett and Nutter, 1970]. River and stream hydrographs from tropical peatland catchments are needed to further explore these hypotheses, but are extremely limited: we are aware only of the data analyzed by Katimon *et al.* [2013]. Consistent with the preliminary predictions here, the weir data from a Malaysian peatland analyzed by Katimon *et al.* [2013] showed peak discharge soon after the end of rainfall events, and a strong effect of antecedent water tables on runoff ratio.

Our scalar model predicts runoff generation in peatland hillslopes, but predicting discharge hydrographs downstream additionally requires a routing model [Lambert, 1972; Beven, 2012]. Besides the obvious importance of geomorphological dispersion from variance in travel times along tributaries [Rinaldo *et al.*, 1991], there are four typical features of rivers draining tropical peatlands that are likely to add complexity to modeling of downstream discharge hydrographs. First, we anticipate an early peak in discharge from overland flow on saturated areas near rivers. Second, details of discharge vs. time will also be affected by tides in many tropical peatland rivers, in which tidal fluctuations are apparent tens to hundreds of kilometers from the coast [Hooijer, 2005; Baum *et al.*, 2007]. Third, tropical convective storms have spatial dimensions of a few kilometers, so heterogeneity or asynchrony of rainfall is likely to be important in larger catchments, and is likely to make rivers overall less “flashy” than the peatland headwaters. And fourth, retardation is likely along banks at high flows, as peatland rivers tend to overflow their channels, leading to

backwater effects [Åkesson *et al.*, 2015]. A scalar model for runoff generation from peat-land subcatchments nonetheless provides a simple building block for inclusion in discharge modeling in tropical catchments, or for estimation of DOC export [Hoyt *et al.*, 2019].

5 Extensions and limitations

5.0.1 Topographic data requirements

Inferring conductivity from recession curves requires accurate topographic information, which is difficult to obtain for tropical peatlands because microtopographic features in the surface are comparable in height to differences in relief that drive flow over kilometers [Hooijer, 2005; Lampela *et al.*, 2016]. LiDAR remains the best currently available approach for characterizing peatland topography, but LiDAR data are not available everywhere, and many important tropical peatlands lack LiDAR coverage completely [for example, in the Congo Basin: Dargie *et al.*, 2017]. Ground surveys are an alternative, but are labor intensive. Of course, any other physically-based approach to hydrologic modeling in tropical peatlands will face similar topographic data requirements.

5.0.2 Catotelm and regional groundwater flows

The water storage in the peat dome comprises storage in the near-surface peat, where the water table actively fluctuates, and deeper, permanently saturated peat. Ingram [1983] referred to these layers as the acrotelm (surface peat) and catotelm (deeper peat), based on a classification used by Soviet scientists [Ivanov, 1981]. Because the catotelm by definition is permanently saturated with water, its water storage is constant and can be ignored in water balance calculations. However, as noted by Siegel [1983], the head difference from the interior to the edge of a dome must drive groundwater flow through the catotelm, possibly extending into subadjacent sediments, from the interior to the exterior of the dome. The flow through the catotelm, although small, must contribute a small “baseflow” to the bounding channels that is a function of the shape and transmissivity of the catotelm.

If a peat dome overlies a more permeable medium, the flow generated by the groundwater mound could extend into the subadjacent formation [Tóth, 1963]. For example, flow through subadjacent sediments has been found to result in complicated seasonal patterns in Glacial Lake Agassiz peatland in Minnesota, USA [Siegel *et al.*, 1995]. Most of the peatlands in Southeast Asia overlie fine mangrove clays, and flow through those clays

is likely to be a negligible contributor to overall water balance. However, some tropical peats overlie sand (in coastal Brunei and some parts of Central Kalimantan, for example), and flow through the subadjacent sand could become an important component of the peatland water balance if the catotelm peat itself does not function as an aquiclude [Ishii *et al.*, 2016]. At least in principle, these regional flow patterns could also be detected via piezometer measurements, although describing the flow patterns would require measurements spanning their spatial scale.

5.0.3 Growing and subsiding peatlands

Peat domes that are not at equilibrium will not have a uniform peat surface Laplacian and will not have strictly uniform water levels. In fact, this is apparent at our site, where the piezometer in the still-growing dome interior has a subtly different master curve from the piezometers where the peat surface Laplacian is uniform [Cobb *et al.*, 2017]. Water table fluctuations are nonetheless uniform in the region of uniform peat surface Laplacian, even though we estimate that the dome interior, further from the river, is still thousands of years away from equilibrium [Cobb *et al.*, 2017].

5.0.4 Drained and degraded peatlands

Extension of our approach to drained and degraded peatlands is important and difficult. Because of the elimination of microtopographic patterning by machinery and fire, and the compaction of surface peat by heavy machinery, the transmissivity profile of the peat is likely to be different in managed and degraded peatlands, as has been observed, for example, in cutover higher-latitude peatlands [Schlotzhauer and Price, 1999; Price, 2003]. In particular, it is likely that the transmissivity profile has a much sharper bend near the peat surface in drained and degraded tropical peats than it does in natural tropical peatlands, as water rises from surface peat that is denser and has a lower conductivity than in natural peatlands into a relatively level duff layer. This will lead to a sharper water-table recession curve, representing much higher transmissivity and possibly saturation overland flow. Infiltration time might not be negligible, both because of lower water tables and because of lower permeability of surface peat. In heavily compacted peatlands, the possibility of Hortonian overland flow also cannot be ruled out. Finally, managed peatlands are also typically divided into blocks of fairly small horizontal extent (20–30 m) separated by field drains, and could begin to approach the limits of the Dupuit-Forchheimer approximation

[Verma and Brutsaert, 1971] if flow through deeper peat is significant. Exploring application of this approach to managed and degraded peatlands will therefore require more empirical work.

5.1 Conclusions

In general, vadose zone dynamics, heterogeneous hydraulic properties and complex topography prevent the amount of water in a hillslope from adequately describing its hydrologic state. However, the master rising and recession curves illustrate that a scalar model can work surprisingly well in predicting water table behavior in tropical peatlands. The similar response of the water table across storms and dry intervals can be explained by the thin vadose zone, special topography and grossly uniform hydraulic properties of natural tropical peatlands. Analysis of the master rising and recession curves can be exploited to obtain a hillslope-aggregated estimate of the hydraulic conductivity profile. In particular, this analysis yields an estimate of the conductivity in the peat surface layer, which is very hard to measure by other means. The conductivity and specific yield profiles obtained from the master curves enables prediction of drydown and drainage in other peatlands with similar vegetation and peat structure but different topography, rainfall and evapotranspiration. Conductivity and specific yield profiles obtained from the master curves could also be valuable as a starting point for distributed-parameter hydrologic models. More work is needed to evaluate how well the scalar approach works in peatlands where the assumptions of the method are not as well satisfied, most importantly peatlands with dense artificial drainage networks and where microtopography has been destroyed. Nonetheless, the scalar approach provides a useful starting point for simulation and hydrologic description of these important environments.

Notation

∇ Gradient operator

$\nabla \cdot$ Divergence operator

ζ Water level relative to the land surface, $\zeta = H - p$

ζ_o Pre-rainfall water level

ζ_* Post-rainfall water level

a, b Coefficients of power-law recession curve per *Kirchner* [2009]

1037	A	Contributing area in a flow tube
1038	c	Contour segment spanning a flow tube
1039	ds	Differential arc length for integrating along a boundary
1040	ET	Evapotranspiration
1041	\overline{ET}	Average evapotranspiration over diurnal cycle
1042	H	Water-table elevation
1043	J_i	Number of time vs. head series defined at head H_i (master recession curves)
1044	k	Discrete water level
1045	\mathbf{n}	Unit normal vector
1046	p	The “land surface,” a smooth surface fit through local minima in the peat surface
1047	P	Cumulative rainfall depth in a storm
1048	Q	Catchment discharge
1049	R	Rainfall intensity
1050	S	Dynamic storage per <i>Kirchner</i> [2009]
1051	S_o	Pre-rainfall storage
1052	S_*	Post-rainfall storage
1053	S_y	Specific yield
1054	T	Transmissivity
1055	t	Time
1056	Δt_j	Time offset for alignment of time vs. head series (master recession curves)
1057	z	Elevation coordinate, positive up

1058 Acknowledgments

1059 We thank Brunei Darussalam Heart of Borneo Centre and the Brunei Darussalam Ministry
 1060 of Primary Resources and Tourism for their support of this project; Hajah Jamilah Jalil
 1061 and Joffre Ali Ahmad of the Brunei Darussalam Forestry Department for facilitation of
 1062 field work and release of staff; Amy Chua for logistical support; Jangarun Eri, Haji Bohari
 1063 bin Idi, Rosaidi Mureh, Alison Hoyt, Laure Gandois, and Sylvain Ferrant for help with the
 1064 original instrument installation, survey and data collection; and Alexandra Konings and
 1065 Jonathan Cobb for critical comments on a draft of this manuscript. We also thank two
 1066 anonymous reviewers, whose comments substantially improved the manuscript. The data
 1067 reported in this paper have been deposited in the PANGAEA open access data archive

[data submission PDI-21849, <https://issues.pangaea.de/browse/PDI-21849>; DOI pending. The data have been uploaded as a supplement to the manuscript for review]. This research was supported by the National Research Foundation Singapore through the Singapore-MIT Alliance for Research and Technology's Center for Environmental Sensing and Modeling interdisciplinary research program and Grant No. NRF2016-ITCOO1-021, and by the USA National Science Foundation under Grant No. 1923478 to C.F.H.

References

- Acreman, M., and J. Holden (2013), How wetlands affect floods, *Wetlands*, 33(5), 773–786, doi:10.1007/s13157-013-0473-2.
- Akbar, R., D. J. S. Gianotti, K. A. McColl, E. Haghighi, G. D. Salvucci, and D. Entekhabi (2018), Estimation of landscape soil water losses from satellite observations of soil moisture, *Journal of Hydrometeorology*, 19(5), 871–889, doi:10.1175/jhm-d-17-0200.1.
- Åkesson, A., A. Wörmann, and A. Bottacin-Busolin (2015), Hydraulic response in flooded stream networks, *Water Resources Research*, 51(1), 213–240, doi: 10.1002/2014wr016279.
- Alkhatib, M., T. C. Jennerjahn, and J. Samiaji (2007), Biogeochemistry of the Dumai River estuary, Sumatra, Indonesia, a tropical black-water river, *Limnology and Oceanography*, 52(6), 2410–2417, doi:10.4319/lo.2007.52.6.2410.
- Anderson, J. A. R. (1964), The structure and development of the peat swamps of Sarawak and Brunei, *Journal of Tropical Geography*, 18, 7–16.
- Anderson, J. A. R. (1983), The tropical peat swamps of western Malesia, in *Mires: Swamp, Bog, Fen and Moor: Regional Studies, Ecosystems of the World*, vol. 4B, edited by A. J. P. Gore, pp. 181–199, Elsevier, Amsterdam, The Netherlands.
- Arnold, J. G., P. M. Allen, R. Muttiah, and G. Bernhardt (1995), Automated base flow separation and recession analysis techniques, *Ground Water*, 33(6), 1010–1018, doi: 10.1111/j.1745-6584.1995.tb00046.x.
- Baird, A. J., P. J. Morris, and L. R. Belyea (2012), The DigiBog peatland development model 1: rationale, conceptual model, and hydrological basis, *Ecohydrology*, 5, 242–255.
- Baird, A. J., A. M. Milner, A. Blundell, G. T. Swindles, and P. J. Morris (2016), Microform-scale variations in peatland permeability and their ecohydrological implications, *Journal of Ecology*, 104(2), 531–544, doi:10.1111/1365-2745.12530.

- 1100 Baird, A. J., R. Low, D. Young, G. T. Swindles, O. R. Lopez, and S. Page (2017), High
 1101 permeability explains the vulnerability of the carbon store in drained tropical peatlands,
 1102 *Geophysical Research Letters*, 44(3), 1333–1339, doi:10.1002/2016GL072245.
- 1103 Baum, A., T. Rixen, and J. Samiaji (2007), Relevance of peat draining rivers in central
 1104 Sumatra for the riverine input of dissolved organic carbon into the ocean, *Estuarine,
 1105 Coastal and Shelf Science*, 73(3-4), 563–570, doi:10.1016/j.ecss.2007.02.012.
- 1106 Bechtold, M., B. Tiemeyer, A. Laggner, T. Leppelt, E. Frahm, and S. Belting (2014),
 1107 Large-scale regionalization of water table depth in peatlands optimized for greenhouse
 1108 gas emission upscaling, *Hydrology and Earth System Sciences*, 18(9), 3319–3339, doi:
 1109 10.5194/hess-18-3319-2014.
- 1110 Beven, K. (2012), *Rainfall–Runoff Modelling*, 2nd ed., Wiley-Blackwell, Chichester, UK.
- 1111 Beven, K., and M. Kirkby (1979), A physically based, variable contributing area
 1112 model of basin hydrology, *Hydrological Sciences Bulletin*, 24(1), 43–69, doi:
 1113 10.1080/02626667909491834.
- 1114 Bidin, K., and N. A. Chappell (2006), Characteristics of rain events at an inland local-
 1115 ity in northeastern Borneo, Malaysia, *Hydrological Processes*, 20(18), 3835–3850, doi:
 1116 10.1002/hyp.6160.
- 1117 Binley, A., K. Beven, and J. Elgy (1989), A physically based model of heterogeneous hill-
 1118 slopes: 2. Effective hydraulic conductivities, *Water Resources Research*, 25(6), 1227–
 1119 1233, doi:10.1029/wr025i006p01227.
- 1120 Boelter, D. H. (1965), Hydraulic conductivity of peats, *Soil Science*, 100(4), 227–231, doi:
 1121 10.1097/00010694-196510000-00001.
- 1122 Bromley, J., M. Robinson, and J. A. Barker (2004), Scale-dependency of hydraulic con-
 1123 ductivity: an example from Thorne Moor, a raised mire in South Yorkshire, UK, *Hydro-
 1124 logical Processes*, 18(5), 973–985, doi:10.1002/hyp.1341.
- 1125 Brutsaert, W., and J. L. Nieber (1977), Regionalized drought flow hydrographs from a
 1126 mature glaciated plateau, *Water Resources Research*, 13(3), 637–643.
- 1127 Center For International Earth Science Information Network–CIESIN–Columbia Uni-
 1128 versity (2017), Gridded population of the world, version 4 (gpwv4): Population den-
 1129 sity adjusted to match 2015 revision of UN WPP country totals, revision 10, doi:
 1130 10.7927/h49884zr, accessed 2019-02-20.
- 1131 Cobb, A. R., A. M. Hoyt, L. Gandois, J. Eri, R. Dommain, K. Abu Salim, F. M. Kai,
 1132 N. S. Haji Su’ut, and C. F. Harvey (2017), How temporal patterns in rainfall deter-

- mine the geomorphology and carbon fluxes of tropical peatlands, *Proceedings of the National Academy of Sciences of the United States of America*, 114, E5187–E5196, doi: 10.1073/pnas.1701090114.
- Dadap, N. C., A. R. Cobb, A. M. Hoyt, C. F. Harvey, and A. G. Konings (2019), Satellite soil moisture observations predict burned area in Southeast Asian peatlands, *Environmental Research Letters*, 14(9), 094,014, doi:10.1088/1748-9326/ab3891.
- Dargie, G. C., S. L. Lewis, I. T. Lawson, E. T. A. Mitchard, S. E. Page, Y. E. Bocko, and S. A. Ifo (2017), Age, extent and carbon storage of the central Congo Basin peatland complex, *Nature*, 542(7639), 86–90, doi:10.1038/nature21048.
- Dettmann, U., and M. Bechtold (2016), Deriving effective soil water retention characteristics from shallow water table fluctuations in peatlands, *Vadose Zone Journal*, 15(10), 1–13, doi:10.2136/vzj2016.04.0029.
- Doherty, J. (2010), *PEST: Model-Independent Parameter Estimation User Manual*, 5th ed., Watermark Numerical Computing.
- Dolan, T. J., A. J. Hermann, S. E. Bayley, and J. Zoltek, Jr. (1984), Evapotranspiration of a Florida, U.S.A., freshwater wetland, *Journal of Hydrology*, 74, 355–371.
- Dommain, R., A. Cobb, H. Joosten, P. Glaser, A. Chua, L. Gandois, F. Kai, A. Noren, K. Abu Salim, S. Su'ut, and C. Harvey (2015), Forest dynamics and tip-up pools drive pulses of high carbon accumulation rates in a tropical peat dome in Borneo (South-east Asia), *Journal of Geophysical Research: Biogeosciences*, 120(4), 617–640, doi: 10.1002/2014JG002796.
- Dooge, J. C. I. (1959), A general theory of the unit hydrograph, *Journal of Geophysical Research*, 64(2), 241–256, doi:10.1029/jz064i002p00241.
- Dunne, T. (1978), Field studies of hillslope flow processes, in *Hillslope Hydrology*, edited by M. Kirkby, pp. 227–293, John Wiley and Sons, Chichester, UK.
- Dunne, T., and R. D. Black (1970), An experimental investigation of runoff production in permeable soils, *Water Resources Research*, 6(2), 478–490, doi: 10.1029/wr006i002p00478.
- Field, R., Y. Wang, O. Roswintarti, and Guswanto (2004), A drought-based predictor of recent haze events in western Indonesia, *Atmospheric Environment*, 38(13), 1869–1878, doi:10.1016/j.atmosenv.2004.01.011.
- Freeze, R. A. (1972), Role of subsurface flow in generating surface runoff: 1. Base flow contributions to channel flow, *Water Resources Research*, 8(3), 609–623, doi:

- 1166 10.1029/wr008i003p00609.
- 1167 Gandois, L., A. Cobb, C. Ing, L. Lim, K. Abu Salim, and C. Harvey (2013), Impact of de-
 1168 forestation on solid and dissolved organic matter characteristics of tropical peat forests:
 1169 implications for carbon release, *Biogeochemistry*, *114*, 183–199, doi:10.1007/s10533-
 1170 012-9799-8.
- 1171 Healy, R. W., and P. G. Cook (2002), Using groundwater levels to estimate recharge, *Hy-
 1172 drogeology Journal*, *10*(1), 91–109, doi:10.1007/s10040-001-0178-0.
- 1173 Heppner, C. S., and J. R. Nimmo (2005), A computer program for predicting recharge
 1174 with a master recession curve, *Scientific Investigation Report 2005-5172*, U.S. Geologi-
 1175 cal Survey.
- 1176 Hewlett, J. D., and W. L. Nutter (1970), The varying source area of streamflow from up-
 1177 land basins, in *Proceedings of the Symposium on Interdisciplinary Aspects of Watershed
 1178 Management*, pp. 65–83, American Society of Civil Engineers, New York, USA.
- 1179 Hidayat, H., D. H. Hoekman, M. A. M. Vissers, and A. J. F. Hoitink (2012), Flood oc-
 1180 currence mapping of the middle Mahakam lowland area using satellite radar, *Hydrology
 1181 and Earth System Sciences*, *16*, 1805–1816, doi:10.5194/hess-16-1805-2012.
- 1182 Hindmarsh, A. C., P. N. Brown, K. E. Grant, S. L. Lee, R. Serban, D. E. Shumaker, and
 1183 C. S. Woodward (2005), SUNDIALS: Suite of nonlinear and differential/algebraic equa-
 1184 tion solvers, *ACM Transactions on Mathematical Software*, *31*(3), 363–396.
- 1185 Hirano, T., J. Jauhiainen, T. Inoue, and H. Takahashi (2009), Controls on the carbon bal-
 1186 ance of tropical peatlands, *Ecosystems*, *12*(6), 873–887.
- 1187 Hoag, R., and J. Price (1995), A field-scale, natural gradient solute transport experiment
 1188 in peat at a Newfoundland blanket bog, *Journal of Hydrology*, *172*(1-4), 171–184, doi:
 1189 10.1016/0022-1694(95)02696-m.
- 1190 Holden, J. (2005), Peatland hydrology and carbon release: why small-scale process mat-
 1191 ters, *Philosophical Transactions of the Royal Society A-Mathematical Physical and Engi-
 1192 neering Sciences*, *363*, 2891–2913.
- 1193 Hooijer, A. (2005), Hydrology of tropical wetland forests: recent research results from
 1194 Sarawak peatswamps, in *Forests, Water and People in the Humid Tropics*, edited by
 1195 M. Bonell and L. A. Bruijnzeel, chap. 17, pp. 447–461, Cambridge University Press,
 1196 Cambridge, UK.
- 1197 Hooijer, A., S. Page, J. Jauhiainen, W. A. Lee, X. X. Lu, A. Idris, and G. Anshari (2012),
 1198 Subsidence and carbon loss in drained tropical peatlands, *Biogeosciences*, *9*, 1053–1071,

- doi:10.5194/bg-9-1053-2012.
- Hoyt, A. M., L. Gandois, J. Eri, F. M. Kai, C. F. Harvey, and A. R. Cobb (2019), CO₂ emissions from an undrained tropical peatland: Interacting influences of temperature, shading and water table depth, *Global Change Biology*, doi:10.1111/gcb.14702.
- Huang, P., S.-P. Xie, K. Hu, G. Huang, and R. Huang (2013), Patterns of the seasonal response of tropical rainfall to global warming, *Nature Geoscience*, 6, 357–361, doi: 10.1038/ngeo1792.
- Ingram, H. (1983), Hydrology, in *Mires: Swamp, Bog, Fen, and Moor, Ecosystems of the World*, vol. 4A, edited by A. Gore, pp. 67–158, Elsevier, Amsterdam, The Netherlands.
- Ishii, Y., K. Koizumi, H. Fukami, K. Yamamoto, H. Takahashi, S. H. Limin, K. Kusin, A. Usup, and G. E. Susilo (2016), Groundwater in peatland, in *Tropical Peatland Ecosystems*, pp. 265–279, Springer Japan.
- Ivanov, K. (1981), *Water Movement in Mirelands*, Academic Press, London, UK, translated from the Russian text *Voddoobmen v blotnykh lanshaftakh* by A. Thomson and H.A.P. Ingram.
- Jepsen, S. M., T. C. Harmon, and Y. Shi (2016), Watershed model calibration to the base flow recession curve with and without evapotranspiration effects, *Water Resources Research*, 52, 2919–2933, doi:10.1002/2015WR017827.
- Kang, S., E.-S. Im, and E. A. B. Eltahir (2019), Future climate change enhances rainfall seasonality in a regional model of western Maritime Continent, *Climate Dynamics*, 52(1-2), 747–764, doi:10.1007/s00382-018-4164-9.
- Katimon, A., S. Shahid, A. K. A. Wahab, and M. H. Ali (2013), Hydrological behaviour of a drained agricultural peat catchment in the tropics. 1: Rainfall, runoff and water table relationships, *Hydrological Sciences Journal*, 58(6), 1297–1309, doi: 10.1080/02626667.2013.815759.
- Kelly, T. J., A. J. Baird, K. H. Roucoux, T. R. Baker, E. N. H. Coronado, M. Ríos, and I. T. Lawson (2014), The high hydraulic conductivity of three wooded tropical peat swamps in northeast Peru: measurements and implications for hydrological function, *Hydrological Processes*, 28(9), 3373–3387, doi:10.1002/hyp.9884.
- Kirchner, J. W. (2009), Catchments as simple dynamical systems: Catchment characterization, rainfall-runoff modeling, and doing hydrology backward, *Water Resources Research*, 45, W02,429, doi:10.1029/2008WR006912.

- 1231 Koster, R. D., R. H. Reichle, and S. P. P. Mahanama (2017), A data-driven approach for
1232 daily real-time estimates and forecasts of near-surface soil moisture, *Journal of Hydrometeorology*, 18(3), 837–843, doi:10.1175/jhm-d-16-0285.1.
- 1234 Kurnianto, S., M. Warren, J. Talbot, B. Kauffman, D. Murdiyarso, and S. Frolking (2015),
1235 Carbon accumulation of tropical peatlands over millennia: a modeling approach, *Global Change Biology*, 21(1), 431–444, doi:10.1111/gcb.12672.
- 1236
1237 Lhteenoja, O., K. Ruokolainen, L. Schulman, and J. Alvarez (2009), Amazonian flood-
1238 plains harbour minerotrophic and ombrotrophic peatlands, *Catena*, 79(2), 140–145, doi:
1239 10.1016/j.catena.2009.06.006.
- 1240 Lambert, A. O. (1969), A comprehensive rainfall/run-off model for an upland catchment
1241 area, *Journal of the Institute of Water Engineering*, 23, 231–238.
- 1242 Lambert, A. O. (1972), Catchment models based on ISO-functions, *Journal of the Institute*
1243 *of Water Engineering*, 26, 413–422.
- 1244 Lampela, M., J. Jauhiainen, I. Kmri, M. Koskinen, T. Tanhuanp, A. Valkeap, and
1245 H. Vasander (2016), Ground surface microtopography and vegetation patterns in a tropi-
1246 cal peat swamp forest, *Catena*, 139, 127–136.
- 1247 Mezbahuddin, M., R. F. Grant, and T. Hirano (2015), How hydrology determines seasonal
1248 and interannual variations in water table depth, surface energy exchange, and water
1249 stress in a tropical peatland: Modeling versus measurements, *Journal of Geophysical*
1250 *Research: Biogeosciences*, 120(11), 2132–2157, doi:10.1002/2015jg003005.
- 1251 Miettinen, J., C. Shi, and S. C. Liew (2016), Land cover distribution in the peatlands of
1252 Peninsular Malaysia, Sumatra and Borneo in 2015 with changes since 1990, *Global*
1253 *Ecology and Conservation*, 6, 67–78, doi:10.1016/j.gecco.2016.02.004.
- 1254 Molengraaff, G. A. F. (1900), *Borneo Expeditie—Geologische Verkenningstochten in*
1255 *Centraal-Borneo (1893–94) (Borneo Expedition - Geological Reconnaissance in Central-*
1256 *Borneo (1893–94)*, H. Gerlings, Amsterdam, The Netherlands.
- 1257 Moore, I. D., and R. B. Grayson (1991), Terrain-based catchment partitioning and runoff
1258 prediction using vector elevation data, *Water Resources Research*, 27(6), 1177–1191.
- 1259 Moore, S., V. Gauci, C. D. Evans, and S. E. Page (2011), Fluvial organic carbon losses
1260 from a Bornean blackwater river, *Biogeosciences*, 8, 901–909, doi:10.5194/bg-8-901-
1261 2011.
- 1262 Morley, R. J. (2013), Cenozoic ecological history of South East Asian peat mires based on
1263 the comparison of coals with present day and Late Quaternary peats, *Journal of Limnol-*

- ogy, 72(s2), 36–59, doi:10.4081/jlimnol.2013.s2.e3.
- Müller, D., T. Warneke, T. Rixen, M. Müller, S. Jamahari, N. Denis, A. Mujahid, and J. Notholt (2015), Lateral carbon fluxes and CO₂ outgassing from a tropical peat-draining river, *Biogeosciences*, 12(20), 5967–5979, doi:10.5194/bg-12-5967-2015.
- Nathan, R. J., and T. A. McMahon (1990), Evaluation of automated techniques for base flow and recession analyses, *Water Resources Research*, 26(7), 1465–1473, doi: 10.1029/wr026i007p01465.
- Page, S., and A. Hooijer (2016), In the line of fire: the peatlands of Southeast Asia, *Philosophical Transactions of the Royal Society B*, 371, 20150176, doi: 10.1098/rstb.2015.0176.
- Posavec, K., A. Bačani, and Z. Nakić (2006), A Visual Basic spreadsheet macro for recession curve analysis, *Ground Water*, 44(5), 764–767, doi:10.1111/j.1745-6584.2006.00226.x.
- Price, J. S. (2003), Role and character of seasonal peat soil deformation on the hydrology of undisturbed and cutover peatlands, *Water Resources Research*, 39(9), doi: 10.1029/2002wr001302.
- Rezanezhad, F., J. S. Price, W. L. Quinton, B. Lennartz, T. Milojevic, and P. V. Cappellen (2016), Structure of peat soils and implications for water storage, flow and solute transport: A review update for geochemists, *Chemical Geology*, 429, 75–84, doi: 10.1016/j.chemgeo.2016.03.010.
- Rinaldo, A., A. Marani, and R. Rigon (1991), Geomorphological dispersion, *Water Resources Research*, 27(4), 513–525, doi:10.1029/90wr02501.
- Ritzema, H., S. Limin, K. Kusin, J. Jauhiainen, and H. Wösten (2014), Canal blocking strategies for hydrological restoration of degraded tropical peatlands in Central Kalimantan, Indonesia, *Catena*, 114, 11–20, doi:10.1016/j.catena.2013.10.009.
- Rodriguez-Iturbe, I., A. Porporato, L. Ridolfi, V. Isham, and D. Cox (1999), Probabilistic modelling of water balance at a point: the role of climate, soil and vegetation, *Proceedings of the Royal Society A-Mathematical Physical and Engineering Sciences*, 455, 3789–3805.
- Romanov, V. (1968), *Hydrophysics of Bogs*, Israel Program for Scientific Translations, Jerusalem, Israel, translated by N. Kaner from *Gidrofizika bolot*, Gimiz Gidrometeorologicheskoe izdatel'stvo, Leningrad, 1961.

- Schlottzhauer, S. M., and J. S. Price (1999), Soil water flow dynamics in a managed cut-over peat field, Quebec: Field and laboratory investigations, *Water Resources Research*, 35(12), 3675–3683, doi:10.1029/1999wr900126.
- Shawki, D., R. D. Field, M. K. Tippet, B. H. Saharjo, I. Albar, D. Atmoko, and A. Voulgarakis (2017), Long-lead prediction of the 2015 fire and haze episode in Indonesia, *Geophysical Research Letters*, 44(19), 9996–10,005, doi:10.1002/2017gl073660.
- Siegel, D. I. (1983), Ground water and the evolution of patterned mires, Glacial Lake Agassiz Peatlands, Northern Minnesota, *The Journal of Ecology*, 71(3), 913, doi:10.2307/2259601.
- Siegel, D. I., A. S. Reeve, P. H. Glaser, and E. A. Romanowicz (1995), Climate-driven flushing of pore water in peatlands, *Nature*, 374(6522), 531–533, doi:10.1038/374531a0.
- Snyder, F. F. (1939), A conception of runoff-phenomena, *Transactions, American Geophysical Union*, 20(4), 725–738, doi:10.1029/tr020i004p00725.
- Surridge, B. W. J., A. J. Baird, and A. L. Heathwaite (2005), Evaluating the quality of hydraulic conductivity estimates from piezometer slug tests in peat, *Hydrological Processes*, 19(6), 1227–1244, doi:10.1002/hyp.5653.
- Takahashi, H., and Y. Yonetani (1997), Studies on microclimate and hydrology of peat swamp forest in Central Kalimantan, Indonesia, in *Biodiversity and Sustainability of Tropical Peatlands*, edited by J. Rieley and S. Page, pp. 179–187, Samara Publishing, Cardigan, UK.
- Taufik, M., P. J. J. F. Torfs, R. Uijlenhoet, P. D. Jones, D. Murdiyarso, and H. A. J. Van Lanen (2017), Amplification of wildfire area burnt by hydrological drought in the humid tropics, *Nature Climate Change*, 7(6), 428–431, doi:10.1038/nclimate3280.
- Tóth, J. (1963), A theoretical analysis of groundwater flow in small drainage basins, *Journal of Geophysical Research*, 68(16), 4795–4812, doi:10.1029/jz068i016p04795.
- Usup, A., Y. Hashimoto, H. Takahashi, and H. Hayasaka (2004), Combustion and thermal characteristics of peat fire in tropical peatland in Central Kalimantan, Indonesia, *Tropics*, 14(1), 1–19, doi:10.3759/tropics.14.1.
- Verma, R. D., and W. Brutsaert (1971), Similitude criteria for flow from unconfined aquifers, *Journal of the Hydraulics Division*, 97(9), 1493–1509.
- Warren, M., K. Hergoualc’h, J. B. Kauffman, D. Murdiyarso, and R. Kolka (2017), An appraisal of indonesia’s immense peat carbon stock using national peatland maps: uncertainties and potential losses from conversion, *Carbon Balance and Management*, 12(1),

- doi:10.1186/s13021-017-0080-2.
- Wells, J. A., K. A. Wilson, N. K. Abram, M. Nunn, D. L. A. Gaveau, R. K. Runting, N. Tarniati, K. L. Mengersen, and E. Meijaard (2016), Rising floodwaters: mapping impacts and perceptions of flooding in Indonesian Borneo, *Environmental Research Letters*, *11*, 064,016, doi:10.1088/1748-9326/11/6/064016.
- White, W. N. (1932), A method of estimating ground-water supplies based on discharge by plants and evaporation from soil: Results of investigations in Escalante Valley, Utah, *Water Supply Paper 659-A*, USGS.
- Wit, F., D. Müller, A. Baum, T. Warneke, W. S. Pranowo, M. Müller, and T. Rixen (2015), The impact of disturbed peatlands on river outgassing in Southeast Asia, *Nature Communications*, *6*(10155), doi:10.1038/ncomms10155.
- World Resources Institute (2018), Peat lands, <http://www.globalforestwatch.org>, accessed through Global Forest Watch on 2018-04-03.
- Xu, J., P. J. Morris, J. Liu, and J. Holden (2018), PEATMAP: Refining estimates of global peatland distribution based on a meta-analysis, *CATENA*, *160*, 134–140, doi: 10.1016/j.catena.2017.09.010.
- Zevenbergen, L. W., and C. R. Thorne (1987), Quantitative analysis of land surface topography, *Earth Surface Processes and Landforms*, *12*, 47–56, doi:10.1002/esp.3290120107.

Figure captions

Figure 1. Schematic of flow and topography in a tropical peatland. **(a)** Peat accumulates over millennia in gently mounded deposits called peat domes. Water flows to the boundaries of a dome through near-surface, high permeability peat (acrotelm) and the permanently saturated peat below (catotelm). **(b)** Portion of a peat dome viewed from above, in a typical setting on an interfluve. **(c)** Portion of a flow tube formed by a groundwater divide, two flowlines, and a contour (c). The Laplacian $\nabla^2 p$ of the peat surface elevation integrated over the closed region A equals the integral of the normal gradient around its boundary. **(d)** Flow tube from (c) in profile view, showing peat surface p (top boundary), water table H (triangle) and their difference $\zeta = H - p$. The magnitude of the gradient in the peat surface elevation $|\nabla p|$ along a contour c is the parameter $\tan \beta$ in the TWI from TOPMODEL. **(e)** The derivative of the integrated peat surface gradient with respect to enclosed area is the average Laplacian of the surface elevation inside the area; the logarithm of this derivative is the reciprocal of the TWI.

Figure 2. Topography of a peat dome in a pristine peatland in Brunei Darussalam. **(a, b)** Location of site in the Belait District of Brunei Darussalam, on the island of Borneo. **(c)** A flow tube from groundwater divide to river at the site based on LiDAR topography, and locations of piezometers (triangles). Contour interval is 10 cm. This flowtube converges to a point on the Malaysian side of the border where LiDAR data are absent (left). **(d)** Profile of flow tube (c), showing positions of piezometers (dotted vertical lines). **(e)** Plot of integrated normal gradient along contour bounding the flowtube versus area enclosed by that contour, as in Figure 1e. [Panels c–e adapted from Figure 6a–c in *Cobb et al.*, 2017].

Figure 3. Water-table recession analysis in a tropical peatland in Brunei Darussalam. **(a)** Average throughfall in four below-canopy rain gauges (piecewise-constant intensity on 20-minute intervals), and **(b)** water level ζ relative to the surface in four shallow piezometers along a 2 km transect (Methods). **(c)** The average water level across the 4 piezometer locations, divided into periods of heavy rain (storms, dark blue) and no rain (interstorm, magenta). **(d, e, f)** Alignment of interstorms into master recession curve by least squares. [Panels b,d adapted from Figure 5a,d in *Cobb et al.*, 2017].

Figure 4. Master rising curve analysis and derivation of hydraulic parameters in a tropical peatland. **(a, b, c)** The water-table response during rain events can be assembled into a rising curve in a similar approach to the water-table recession analysis (Figure 3). The

water level before and after each storm and the storm depth are represented by line segments that are then aligned by least squares to construct a single master rising curve (**c**) that links the water dynamically stored in the soil and the water level relative to the peat surface. The master rising curve in combination with the master recession curve (**d**) can be used to determine the bulk hydraulic properties of the peat effectively averaged over a large area. The specific yield (**e**) is the inverse of the derivative of the master rising curve (**c**), and the discharge and transmissivity (**f**) can be obtained from the recession curve and the specific yield using the Laplacian of the peat surface elevation (see Figures 1 and 2). The transmissivity is parameterized by a piecewise linear function for the logarithm of conductivity (derivative of transmissivity with respect to water level; **g**). (**h**) Empirical cumulative distribution of water level averaged across piezometers (see Figure 3c), and histogram (normalized to fill panel). [Panels c–f adapted from Figure 5e,f,b,c in *Cobb et al.*, 2017].

Figure 5. A typical explicit-soil-moisture-accounting (ESMA) model (left) compared to the scalar model we describe for a tropical peatland in its equilibrium topography (right).

Figure 6. How the storm response of a tropical peatland in equilibrium can be read off master rising and recession curves without hydrologic parameterization. A particular pattern of storms (**a**) drives a water-table response (**b**). Because of the special topography of an equilibrium peatland, the water table responds in a consistent way to rain and dry intervals, represented by the master rising (**c**) and recession curves (**d**), and in fact this response can be effectively read off of the master curves. When a rain storm of depth P occurs (1), we read the final position of the water table (2) from the rising curve by finding the point on the curve that has P greater dynamic storage than the initial water table. Then, we follow the recession curve (**d**) down for the duration of the dry interval, giving us the water level at the start of the next storm (3). We then repeat the process to determine the water level through the next storm (4, 5). Once hydrologic parameterization has been performed by fitting the master curves (Figure 5), the response of the water table can also be interpreted in terms of the fluxes (**e**) and cumulative fluxes (**f**) through each storm event.

Figure 7. Scalar dynamics of near-equilibrium peatland hillslope in Brunei Darussalam derived from master rising and recession curves. (**a**) Computed discharge Q vs. dynamic storage S , describing the rainfall-runoff response of this peatland hillslope. (**b**) Computed

recession dQ/dS vs. discharge Q based on parameterization from Brunei site. The deviation at lower discharge from the behavior predicted by *Kirchner* [2009] of an exponential store (dashed line) arises mostly because of evapotranspiration, as discussed by *Jepsen et al.* [2016].

Figure 8. Effect of antecedent moisture on computed storm response of tropical peatlands. (a) Time “constant” of computed recession of discharge (equation 10) given different antecedent moisture (dynamic storage) in a tropical peatland. (b) Computed discharge vs. time from a design storm of 20 mm / h intensity and 2 h duration with different initial discharge. Note the contrast with a unit hydrograph model, in which a higher initial discharge would simply shift the storm response vertically because of the principle of superposition (linearity). (c, d) Calculated peak discharge during design storms with different antecedent moisture (pre-event discharge or pre-event water level). Solid lines: 10 mm / h; dashed lines: 20 mm / h; total depths 20, 40 and 60 mm.

Figure 9. Effect of intermittency of rainfall on calculated peak discharge. Mean 95th percentile of calculated peak hillslope discharge versus statistics of a simple model of rainfall, in which storms are modeled as impulses with exponentially distributed depths arriving as a Poisson process. The vertical axis represents increasing average mean net precipitation (rainfall – evapotranspiration), whereas the horizontal axis represents increased intermittency in rainfall (mean time between rain storms) at the same mean net precipitation.

Figure 1.

Author Manuscript

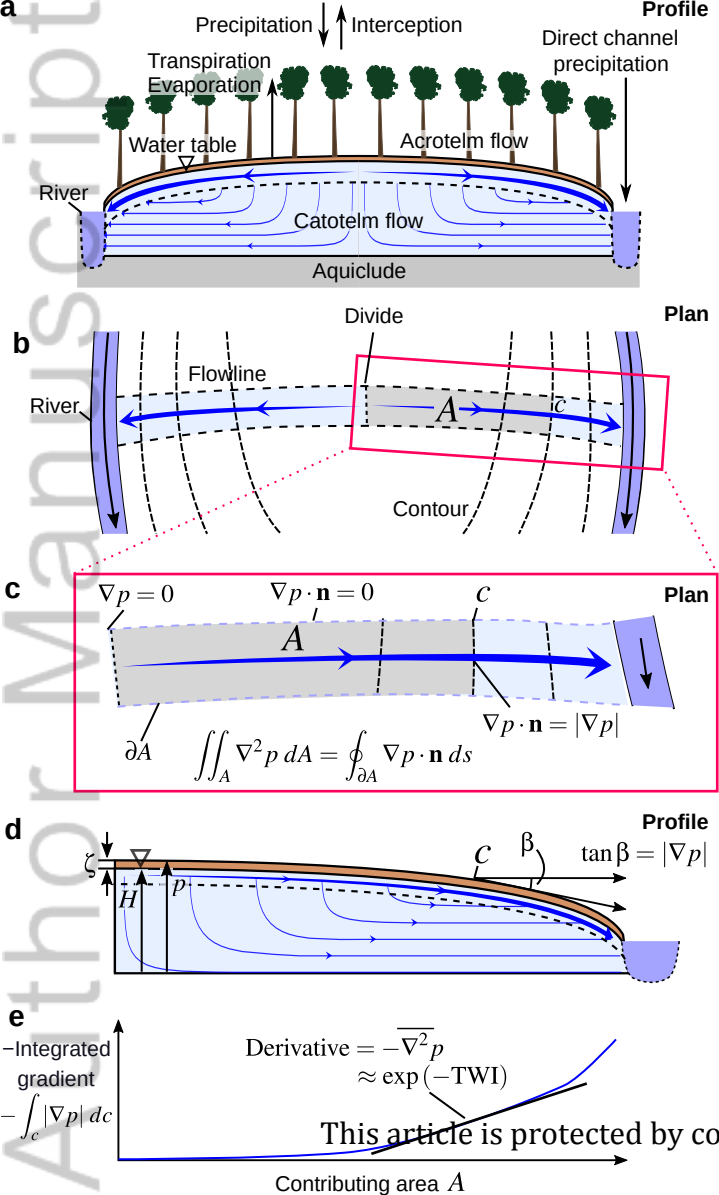


Figure 2.

Author Manuscript

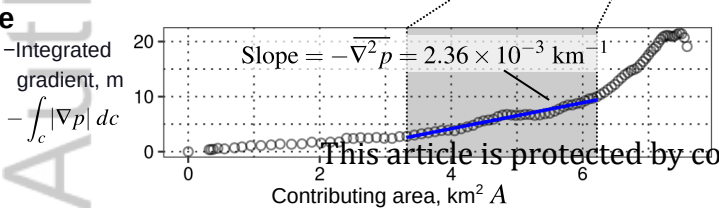
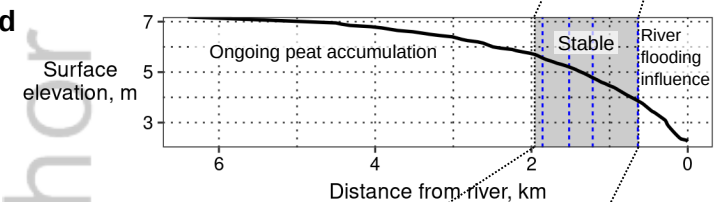
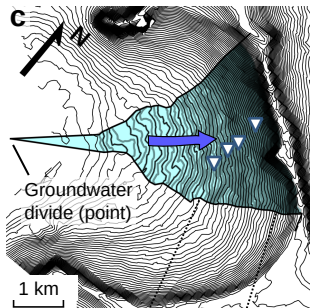
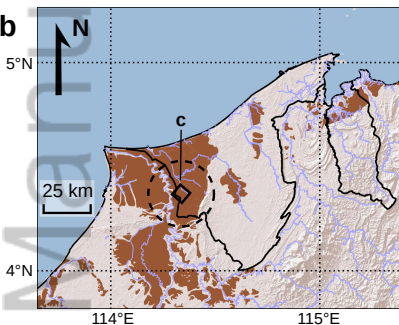
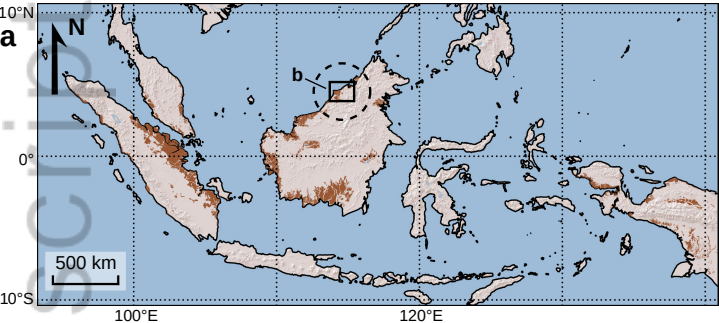


Figure 3.

Author Manuscript

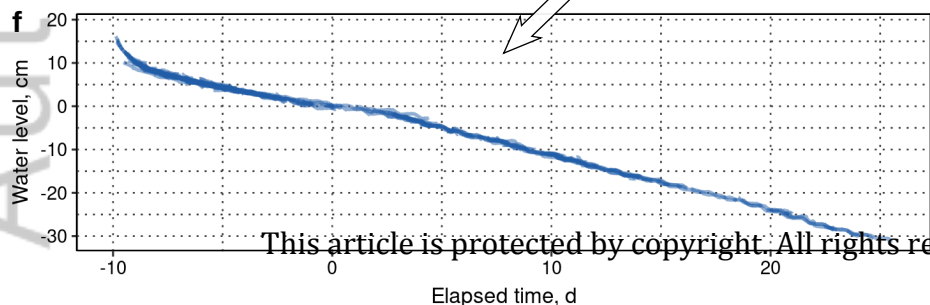
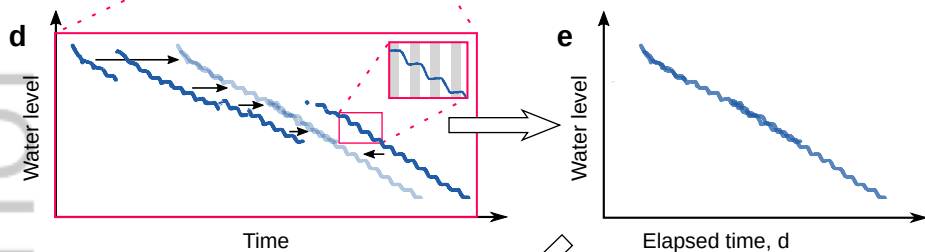
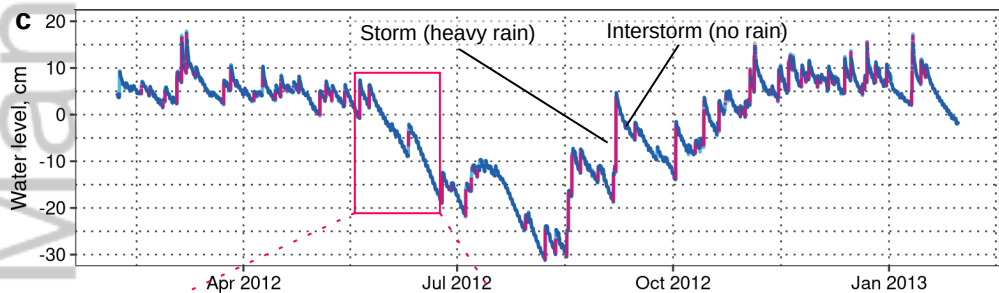
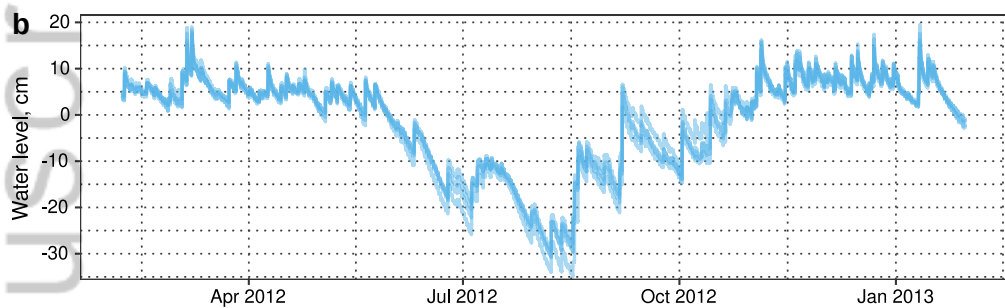
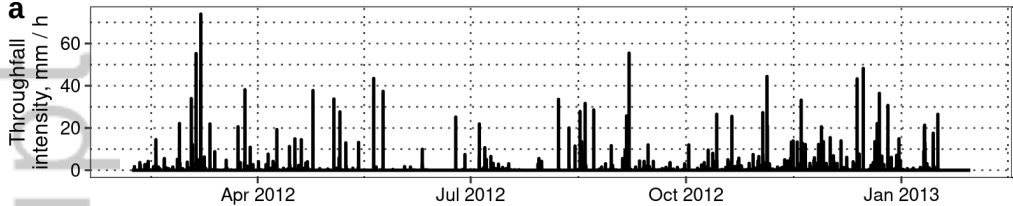


Figure 4.

Author Manuscript

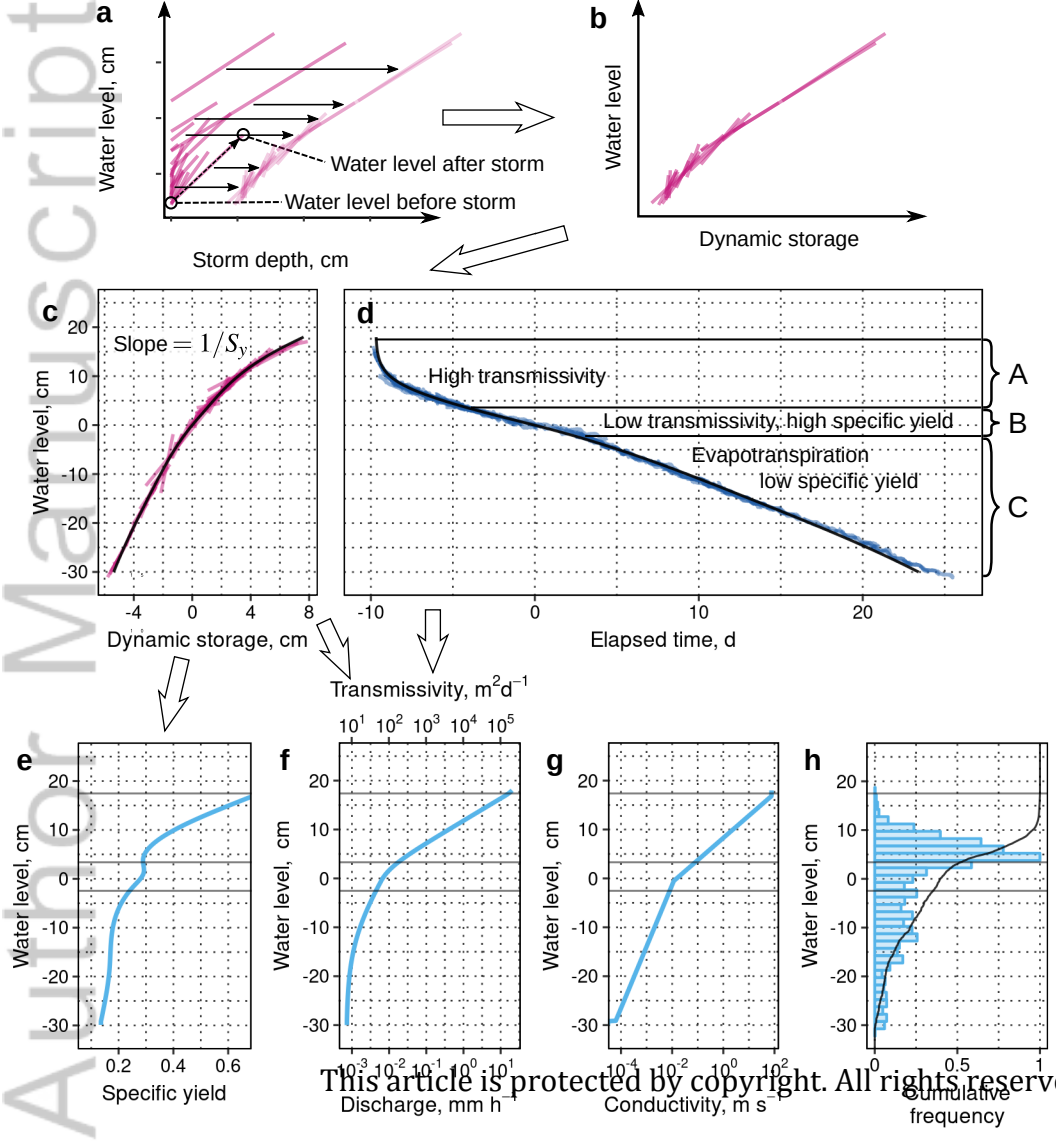
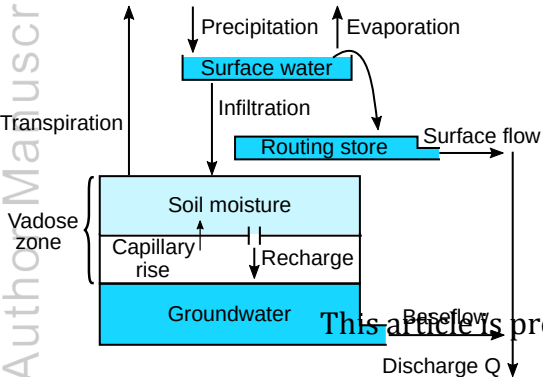


Figure 5.

Author Manuscript

Structure of typical ESMA model



Structure of tropical peatland model

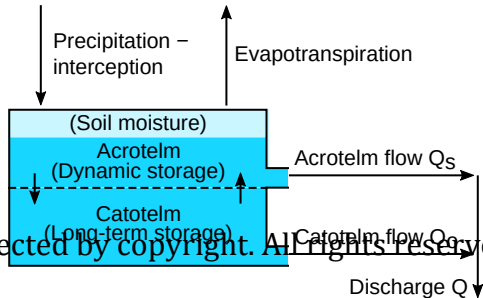


Figure 6.

Author Manuscript

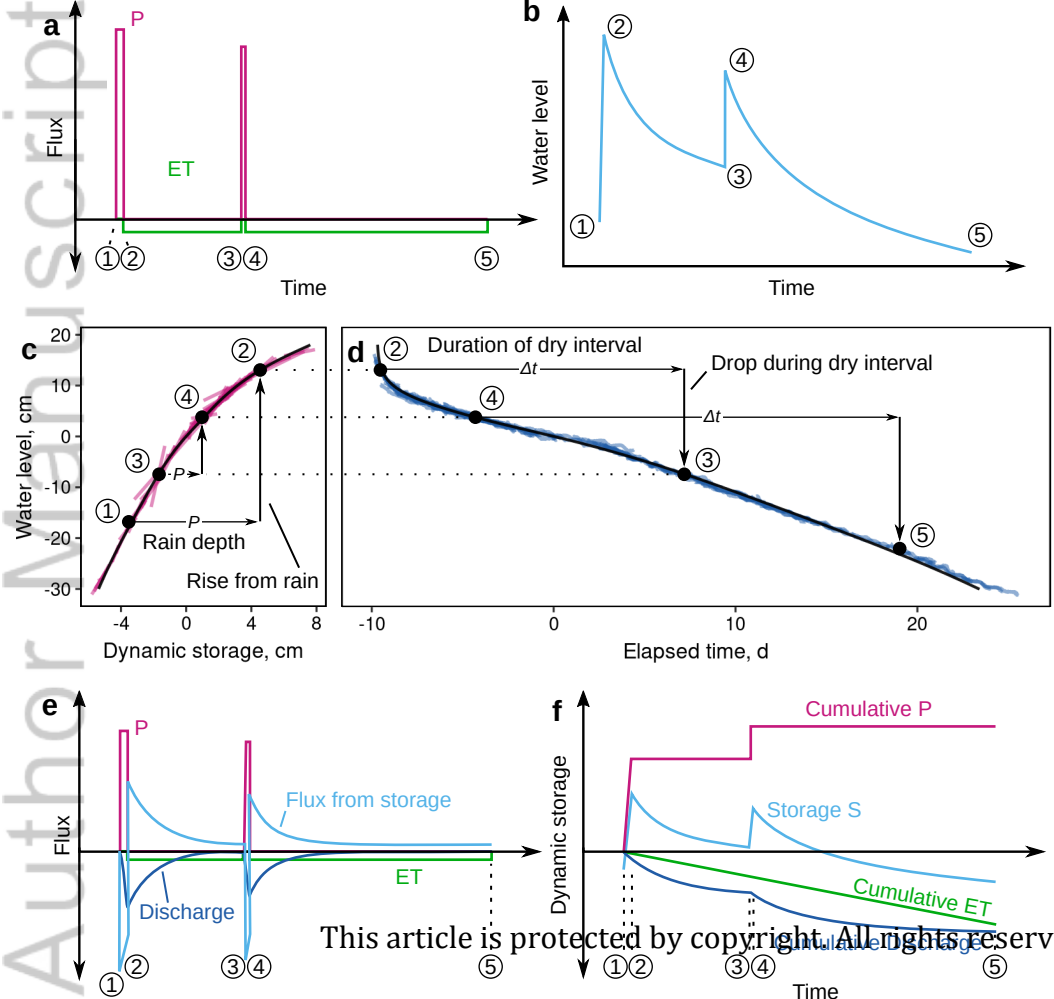


Figure 7.

Author Manuscript

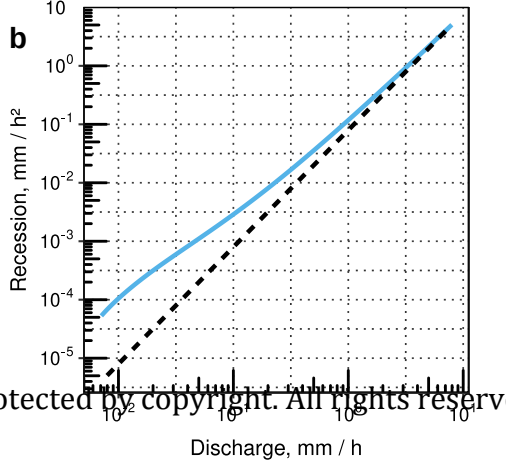
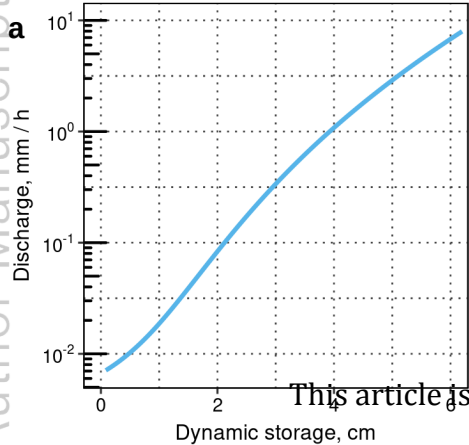


Figure 8.

Author Manuscript

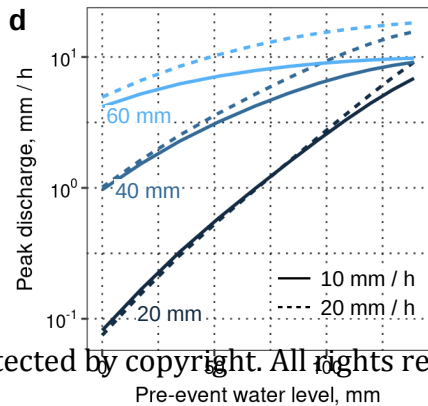
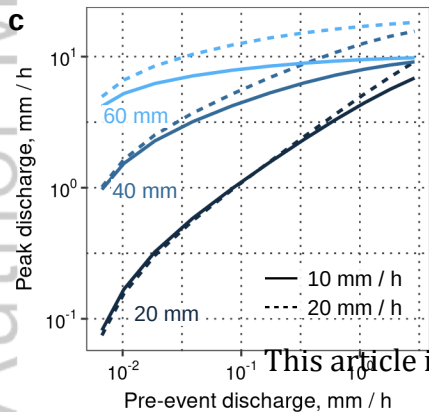
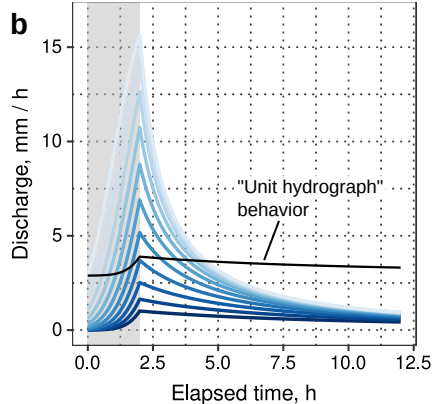
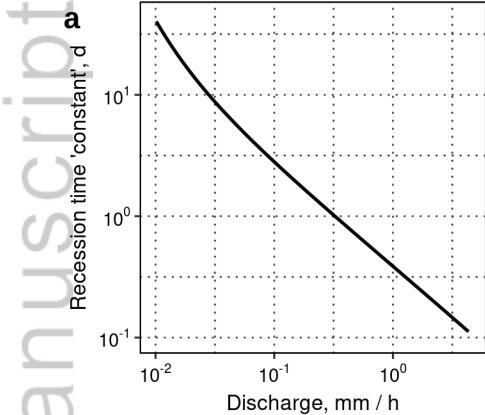
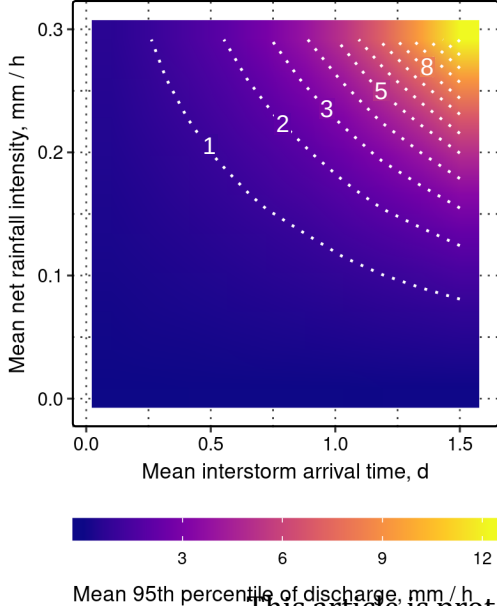
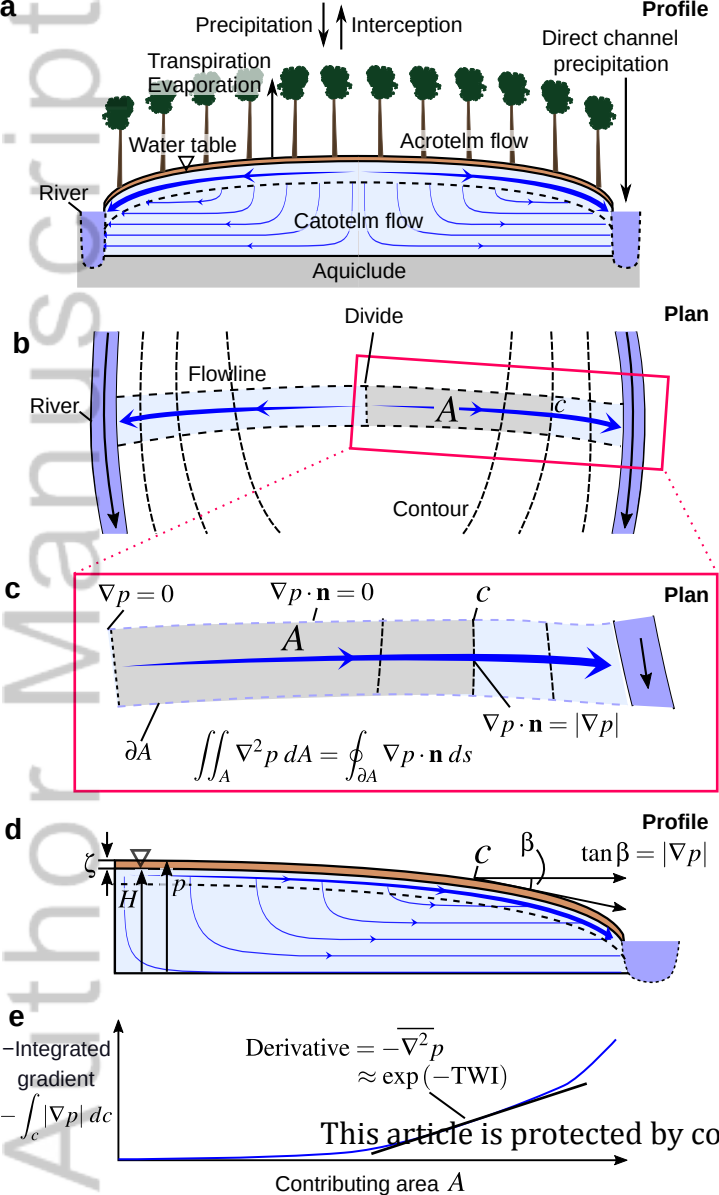
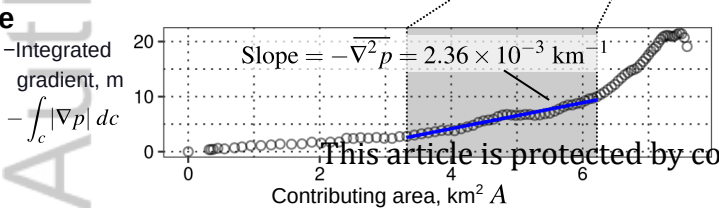
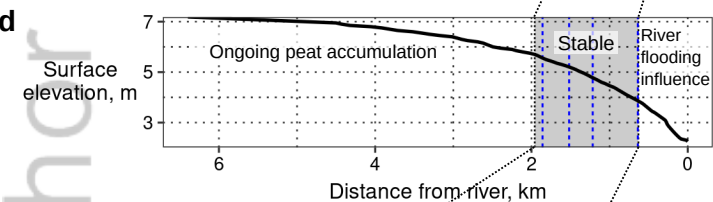
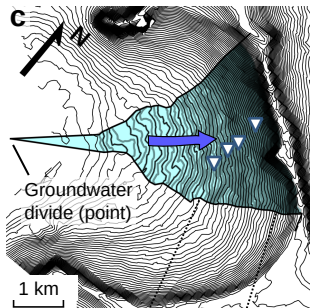
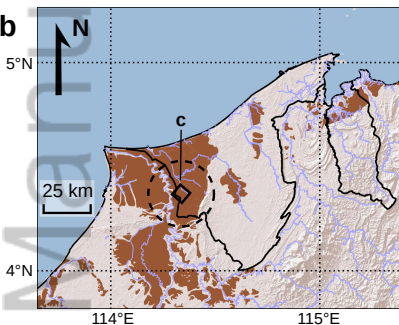
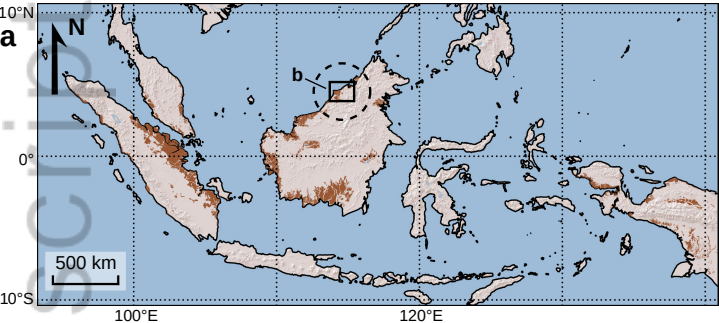


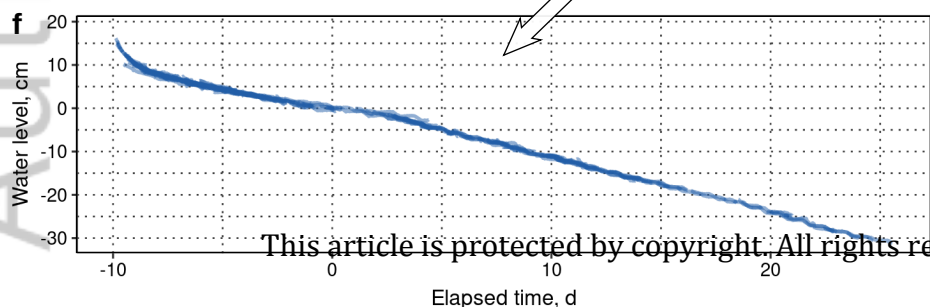
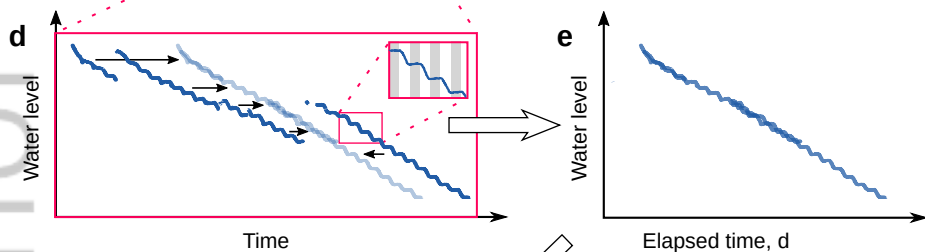
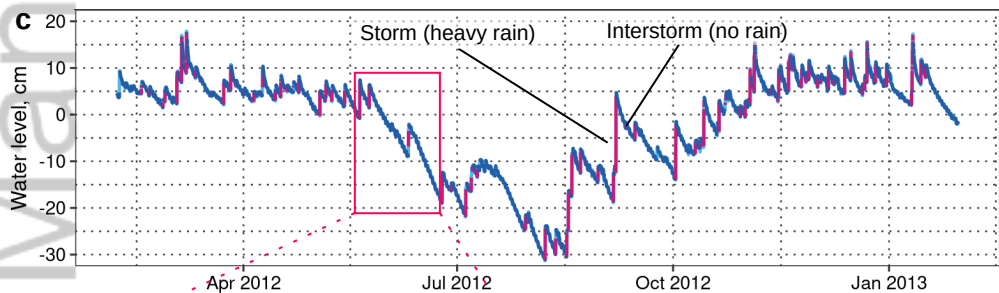
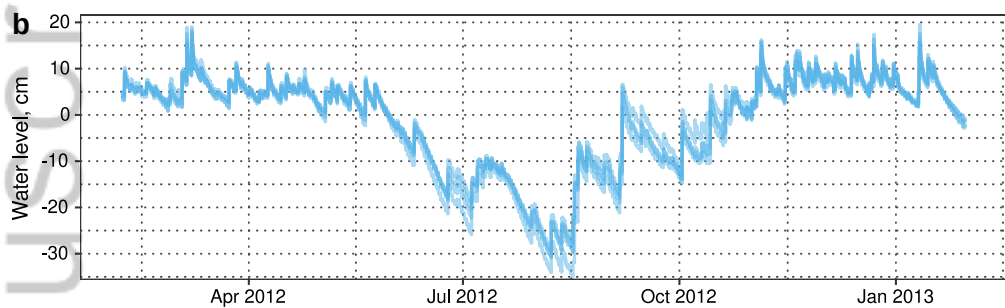
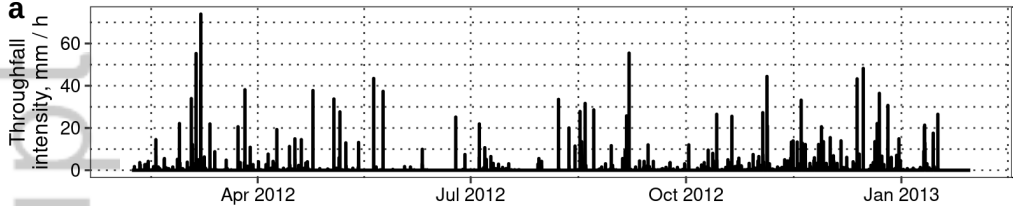
Figure 9.

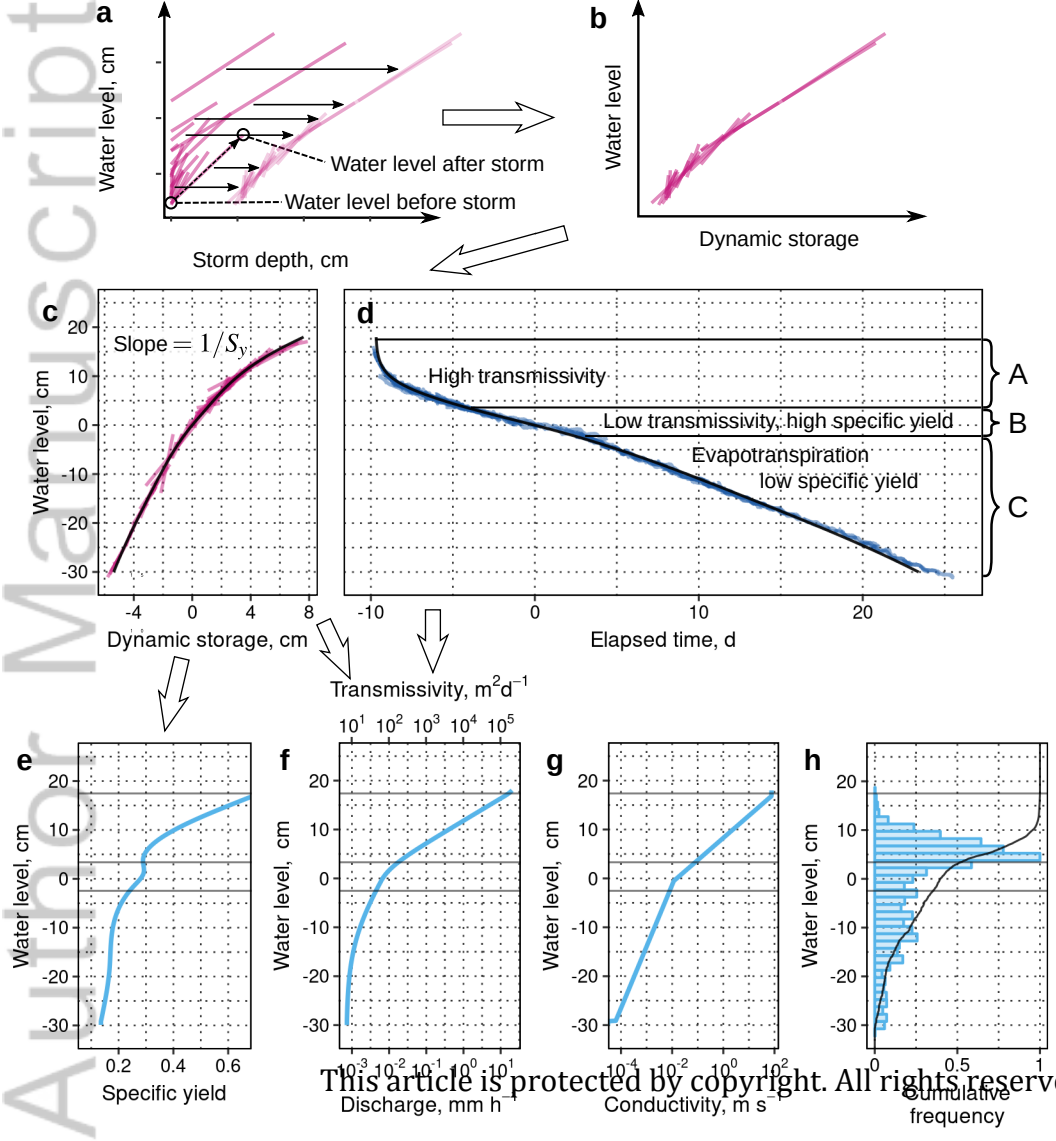
Author Manuscript



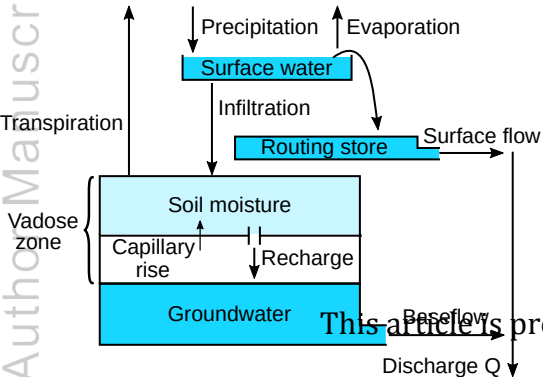








Structure of typical ESMA model



Structure of tropical peatland model

